DOCTOR OF PHILOSOPHY

Multimodal Magnetic Resonance Investigation of Neurovascular Uncoupling in Hypoxia

Rogan, Matthew

Award date:
2024

Awarding institution:
Bangor University

Bangor University

Multimodal Magnetic Resonance Investigation of Neurovascular Uncoupling in Hypoxia

Matthew Rogan

Thesis submitted to the School of Human and Behavioural Sciences, Bangor University, in fulfilment of the requirements for the degree of Doctor of Philosophy

May 2024

‘I hereby declare that this thesis is the results of my own investigations, except where otherwise stated. All other sources are acknowledged by bibliographic references. This work has not previously been accepted in substance for any degree and is not being concurrently submitted in candidature for any degree unless, as agreed by the University, for approved dual awards.

I confirm that I am submitting this work with the agreement of my Supervisor(s).’

‘Yr wyf drwy hyn yn datgan mai canlyniad fy ymchwil fy hun yw’r thesis hwn, ac eithrio lle nodir yn wahanol. Caiff ffynonellau eraill eu cydnabod gan droednodiadau yn rhoi cyfeiriadau eglur. Nid yw sylwedd y gwaith hwn wedi cael ei dderbyn o’r blaen ar gyfer unrhyw radd, ac nid yw’n cael ei gyflwyno ar yr un pryd mewn ymgeisiaeth am unrhyw radd oni bai ei fod, fel y cytunwyd gan y Brifysgol, am gymwysterau deuol cymeradwy.

Rwy'n cadarnhau fy mod yn cyflwyno'r gwaith hwn gyda chytundeb fy Ngoruchwyliwr (Goruchwylwyr)

Acknowledgements

I want to thank my supervisory team, namely Professor Paul Mullins, Professor Jamie Macdonald and Professor Sam Oliver. All have provided me with countless hours of support, guidance and encouragement throughout this PhD studentship.

I particularly want to single out Paul who throughout the years has never failed to demonstrate compassion and care towards myself. He has always shown a real zest and rigour for the task at hand, topic we are delving into or field we seek to contribute. Attributes and practices I can only hope to take forward with me.

I would like to thank all other colleagues I met throughout the course of my studies. Many of whom I am now fortunate to call friends who I will remain in contact with for the foreseeable. I look back fondly on the many hours spent alongside my good friend and office mate Eva, her company never failed to spur me along. I would like to thank Joe, he and I started this journey together and over time working in Pauls lab we have become the best of friends. I will be forever grateful for the opportunity to work alongside him and have made more than enough memories to last a lifetime.

Finally, as I write this, I think about my family, those still with us and the others who have gone yonder over the course of this journey. They have shown unwavering support and trust in whatever I embark upon. Although, it always makes me giggle that at times, they still cannot completely fathom what I have been doing in North Wales for the last 9 years

Table of Contents

List of Figures

List of Tables

List of Abbreviations

APT	Amide Proton Transfer Imaging
AMS	Acute Mountain Sickness
ASL	Arterial Spin Labelling
ATT	Arterial Transit Time
BASIL	Bayesian Inference for Arterial Spin Labelling Magnetic Resonance Imaging
BET	Brain Extraction Tool
BIU	Bangor Imaging Unit
BOLD	Blood Oxygen Level Dependant Imaging
CBF	Cerebral Blood Flow
CDO_2	Cerebral delivery of oxygen to the tissues
CEST	Chemical Exchange Saturation Transfer Imaging
CHESS	Chemical Shift Selective Fat Saturation
Cho	Choline
$CMRO_2$	Cerebral Metabolic Rate of Oxygen
CO_2	Carbon Dioxide
Cr	Creatine
DMN	Default Mode Network
D’	Signal Detection Theory Indices dprime
ECG	electrocardiogram
FAST	FMRIB’s Automated Segmentation Tool
^{18}FDG-PET	2-[^{18}F]deoxy-2-fluoro-D-glucose positron-emission tomography
FID	Free Induction Decay
F_iO_2	Fraction of Inspired Oxygen
FLIRT	FMRIBs Linear Image Registration Tool
FMRIB	Oxford Centre for Functional Magnetic Resonance Imaging of the Brain
fMRS	Functional Magnetic Resonance Spectroscopy
FOV	Field of View
FSL	FMRIB Software Library
FWHM	Full Width at Half Maximum
GABA	gamma-aminobutyric acid
gCBF	Global Cerebral Blood Flow
Glx	Glutamate + Glutamine

GSH	Glutathione
h	Hour
Hz	Hertz
jMRUI	Java-based version of the magnetic resonance user interface
L	Litre
Lac	Lactate
LLQ	Lake Louise Questionnaire
m	Meters
mI	myo-inositol
mL	Millilitre
mm	Millimetres
mm^3	Millimetres Cubed
MNI	Montreal Neurological Institute
MRI	Magnetic Resonance Imaging
MRS	Magnetic Resonance Spectroscopy
MP-RAGE	magnetization-prepared 180 degrees radio-frequency pulses and rapid gradient-echo
ms	Milliseconds
NAA	N-acetylaspartate
$PaCO_2$	Partial pressure of carbon dioxide within the blood
PaO_2	Partial pressure of oxygen within the blood
PCC	Posterior Cingulate Cortex
$P_{ET}CO_2$	Partial Pressure of End-Tidal Carbon Dioxide
PRESS	Point Resolved Spectroscopy
QUEST	Quantification based on quantum estimation
QUIPSS II	Quantitative imaging of perfusion using a single subtraction, second version
RANDOMISE	FSL's tool for nonparametric permutation inference on neuroimaging data
RT	Reaction Time
S	Seconds
SENSE	Sensitivity Encoding
SNR	Signal to Noise Ratio
S_PO_2	Oxygen Saturation
T	Tesla
TE	Echo Time

TR	Repetition Time
TTL	Transistor-transistor Logic
T_1	Spin-lattice (longitudinal) relaxation time of nucleus.
T_2	Spin-lattice (transverse) relaxation time of nucleus.
T_{2*}	Apparent transverse relaxation
2AFC	Two Alternative Forced Choice Task
3D	Three Dimensions
^1H	Hydrogen Nuclei, Proton
^1H-MRS	Proton Magnetic Resonance Spectroscopy
HERMES	Hadamard Encoding and Reconstruction of MEGA-Edited Spectroscopy

Thesis Summary

Being exposed to a hypoxic environment causes a desaturation in the arterial oxygen content. In response to this, breathing and heart rate will be enhanced, and vascular smooth muscle will relax facilitating vasodilation. Overall, this maintains the delivery of oxygen to the cerebral tissue to suffice metabolic demand, despite the prevailing hypoxic environment. Paradoxically, some regions of the brain display a reduced perfusion during hypoxia. Particularly the posterior cingulate cortex, a major node of the default mode network, has consistently shown a reduction in perfusion during hypoxia. Furthermore, during memory recall, a function this region is explicitly involved in, hypoxia reversed the task induced BOLD response within this region. The observations in both the resting and functional brain suggest that hypoxia reverses neurovascular coupling.

This thesis contains three experiments designed to measure the functional, metabolic, and vascular changes to hypoxia on a regional level within the brain. With the aim of elucidating whether or not there is alteration in neurovascular coupling.

We have shown that hyperventilation induced hypocapnia during hypoxia and the resulting state of tissue alkalosis does not drive the reduction in regional cerebral blood flow. Hypoxia negates the increase in posterior cingulate glutamate during task. It is believed this reflects a regional shift towards non-oxidative metabolism in the absence of sufficient regional cerebral blood flow to meet metabolic demands. Resting levels of the inhibitory neurotransmitter GABA, are increased within the posterior cingulate cortex during hypoxia. This is indicative of an increased inhibitory tone within the region. Taken together, the reductions in blood flow and markers of enhanced non-oxidative metabolism suggest there is a state of neurovascular uncoupling during hypoxia. An up-regulation of regional inhibition may be contributing to this, however, it is unclear if increased GABA concentrations is a cause or effect of neurovascular uncoupling during hypoxia; this hypothesis requires further investigation.

This thesis provides a comprehensive investigation of the vascular, metabolic and neuroactivity changes in the brain during hypoxic stress. It adds to the ever-expanding body of research that aims to understand the functioning of the brain in health, disease and during environmental extremes.

Chapter 1
General Introduction

1.1 Introduction

Humans are well adapted for life at sea level, where oxygen is present as 21 % of the atmosphere, however, they do not stay at sea level, and often venture into regions of differing altitudes, both above, and below, sea level, where conditions and oxygen content vary greatly. Sometimes, these excursions are of short duration, for recreation (e.g mountaineering, hiking, or skiing), exploration (mountaineering, space travel) or work (pilots, engineers, astronauts), and at others they may be more prolonged due to migration and settling at higher altitudes. As such understanding how the human body copes with the changes in oxygen availability in these differing environments has been extensively studied, and while we know a lot about how the body does respond to alterations in oxygen content, there is still much to learn. This PhD Thesis will describe three experiments that were performed to investigate the responses of cerebral physiology to a semi-acute hypoxic environment.

1.1.1 Environmental hypoxia and hypoxaemia

At sea level oxygen comprises 21% of the air mixture, with increasing altitude the barometric pressure decreases, which results in a reduction in the partial pressure of oxygen (PO_2) (Milroy, 2018). At 1500 meters (m) above sea level, the effective level of oxygen in the air will fall to 17.3%, 14.4% at 3000m and 11.2% at 5000m (Milroy, 2018).

Within seconds of being exposed to, and breathing within a hypoxic environment, hypoxaemia ensues and there is an almost immediate augmentation of ventilatory activity (Pamenter & Powell, 2016), termed the hypoxic ventilatory response (HVR). As arterial oxygen saturation (Sa_{O2}) decreases, peripheral arterial chemoreceptors (principally at the carotid bodies) are sensitive to this change, which inevitably stimulate the respiratory motor neurons and increase ventilation via excitation of the phrenic nerve (Pamenter & Powell, 2016). In addition to enhanced ventilation, heart rate also increases and mean arterial pressure (Ainslie & Poulin, 2004; Hanada, Sander & González-Alonso, 2003). When hypoxaemia is sustained, beyond 5 minutes and at least to 20 minutes, there will be a decrease in ventilation below the level that had been achieved during the preceding acute HVR. This Hypoxic Ventilatory Decline (HVD) lasts until Ventilatory Acclimatisation to Hypoxia (VAH) occurs with days to weeks of continued exposure to environmental hypoxia (Pamenter & Powell, 2016).

The hypoxia induced hyperventilation results in a reduction in arterial carbon dioxide (Pa_{CO2}). This state of hypocapnia is dependent on the degree of pulmonary ventilation and

depending on its degree, it can cause considerable changes in acid base status, particularly a shift towards a state of alkalosis (Swenson, 2016). This respiratory alkalosis will blunt the adaptive process that have been initiated by and are designed to limit the effect of hypoxaemia (Swenson, 2016). One particular effect of alkalosis, is the blunting of vasodilation, limiting the enhancements in cerebral blood flow (Fan et al., 2010). Thus, poikilocapnic hypoxia allows for the co-occurrence hypoxaemia driving vasodilation, and hypocapnia, driving vasoconstriction.

1.1.2 Global and regional cerebral blood flow and environmental hypoxia

Upon exposure to hypoxia, vasodilation reduces cerebrovascular resistance and increases global cerebral blood flow (Cohen et al., 1967; Kety & Schmidt, 1947). This has been a consistent observation and is achieved through a dilatory response transcending the vascular tree, from the pial vessels (Wolff, Lennox & Allen, 1930), to the larger intracranial arteries (middle cerebral artery) (Imray et al., 2014; Willie et al., 2014), and extracranial conduit arteries (Internal carotid and vertebral arteries) (Lewis et al., 2014). The compensatory increases in cerebral blood flow that accompany this vasodilation, may offset the reduction in arterial oxygen saturation and preserve the delivery of oxygen to cerebral tissues.

However, the compensatory increase in cerebral blood flow during hypoxia is not uniform across the brain. Cerebral blood flow to the posterior regions of the brain or brain stem have been shown to be more reactive to hypoxia than arteries serving other regions of the brain (Ogoh et al., 2013; Willie et al., 2012), and on a regional level, the increases in CBF have been reported to be non-uniform (Rossetti et al. 2020; Lawley et al., 2017; Nöth et al., 2008). Particularly, the posterior cingulate cortex (PCC) has repeatedly displayed reduced perfusion during hypoxia.

1.1.3 Global and regional cerebral metabolism and environmental hypoxia

Upon exposure to hypoxia, global CBF (gCBF) increases concomitantly with falling arterial oxygen saturations (Ainslie & Subudhi, 2014). The increase in gCBF is hypothesised to maintain the cerebral delivey of oxygen (CDO_2) sustaining the global cerebral metabolic rate of oxygen ($CMRO_2$) (Ainslie et al., 2014).

When measured globally, cerebral metabolism has been found to increase (Smith et al., 2013; Vestergaard et al., 2016; Wang et al., 2015), decrease (Jensen et al., 2018) or be unchanged (Vestergaard & Larsson, 2019) during periods of acute poikilocapnic hypoxia.

Regional investigations of cerebral metabolism are less common and have utilised variations of intensities and durations of the hypoxic stimulus. Of such investigations, Hochachka et al. (1996) demonstrated that whole brain regional cerebral glucose metabolism in the brains of Tibetan high-altitude natives did not significantly differ from that observed in lowlanders using 2-[^{18}F]deoxy-2-fluoro-D-glucose positron-emission tomography (^{18}FDG-PET). However, the phylogenetically younger, less well adapted, high altitude dwelling Quechua natives, displayed a near uniform reduction in regional cerebral metabolism compared to the two latter groups (Hochachka et al., 1996). Furthermore, lowlanders who travel to high altitude have demonstrated both reductions and increases in regional metabolism (Hochachka et al., 1999; Merz et al., 2006). The authors conclude that the reduction in regional cerebral metabolism may serve as a defence mechanism in the face of hypoxia, akin to that observed in hypoxia-adapted vertebrates (Hochachka et al., 1996; Hochachka et al., 1999).

Several previous studies reporting increases in cerebral lactate over varying severities of the hypoxic stimulus and durations (Edden et al., 2010; Jensen et al., 2018; Vestergaard et al., 2016; Vestergaard & Larsson, 2019). Furthermore, it has been shown that the increases in cerebral lactate measured by MRS do reflect increases in lactate generated within cerebral tissues, rather than being explained by a systemic increase in lactate during exposure to environmental hypoxia (Vestergaard et al., 2016; Harris et al., 2013).

The origins of the hypoxia-induced increase in cerebral lactate are somewhat unknown. Increased lactate has been hypothesised to reflect an up regulation of anaerobic mechanisms to meet enhanced energy demands during hypoxia when $CMRO_2$ has been observed to increase (Vestergaard et al., 2016). However, numerous other investigations have shown $CMRO_2$ to remain stable during hypoxia, suggesting enhancements in global cerebral blood flow maintain cerebral oxygen delivery to meet demand (Ainslie et al., 2014). Despite this stability, lactate concentration across the brain still increases (Vestergaard et al., 2022; Vestergaard & Larsson, 2017; Ainslie et al., 2014). This suggests the increase in lactate results from an upregulation of glycolysis in response to hypoxia as an alternative, anaerobic metabolic process in the face of low oxygen availability (Vestergaard et al., 2022).

1.1.4 Functioning human brain and hypoxia

To further investigate a possible change in metabolic coupling, a recent investigation by Rossetti et al. (2020) utilising a memory association task, revealed an alteration in the task-induced BOLD responses during hypoxia. Specifically, regions that during normoxia showed a positive BOLD signal in response to the task reversed, showing a negative BOLD

signal in hypoxia, and the opposite also happened – whereby a task induced negative BOLD in normoxia became a positive BOLD response in hypoxia (Rossetti et al., 2020). Generally, negative BOLD measures are interpreted to suggest regions where neural activity has been actively suppressed. However, inversion of the BOLD response to task-based neural activation has been observed in the brains of neonates (Kozberg & Hillman, 2016) and rat models exposed to anaesthesia (Sharp et al., 2015) indicating that the mechanisms of the negative BOLD response may depend on the specific temporal characteristics and metabolic conditions involved. The findings of Rossetti et al. (2020) suggest hypoxia is another such metabolic condition. The unusual haemodynamic response in these conditions is hypothesised to be the result of neural activation stimulating local vasoconstriction, impeding CBF delivery, in a reversal of standard neurovascular coupling (Rossetti et al., 2020). Nevertheless, without an alternative to using BOLD as a measure of metabolism, or neural activity, this is still only conjecture, requiring further investigation.

1.1.5 The posterior cingulate cortex

The PCC is located at the caudal end of the cingulate gyrus within the medial parietal cortex. To the superior of the PCC lies the precuneus and it's inferior, the retro splenial cortices (Leech & Smallwood, 2019). The PCC and neighbouring precuneus are regions of high baseline metabolism, in comparison to other regions of the brain. The PCC is among brain regions with the highest levels of cerebral glucose metabolism (Vogt & Laureys, 2005) it boasts an average a 40% greater blood flow than the regional average (Leech & Smallwood, 2019; Raichle et al., 2001). The metabolic turnover of the PCC is responsive to cognitive state, with cognitive exertion resulting in a 6% perturbation of perfusion (Pfefferbaum et al., 2011). This uniquely high baseline rate of metabolism is indicative of one the PCCs functions as being involved in arousal state, its activation and metabolism vary with level of arousal (Boly et al., 2008; Leech & Sharp, 2014). Increased activity is also associated with the retrieval of autobiographical memories or thinking of the future (Leech & Sharp, 2014). The PCC is also thought to serve a moderator role for the regulation of attentional focus (Gusnard & Raichle, 2001; Hahn, Ross & Stein, 2007), particularly regulating the balance between internally directed thought and externally focused attention (Leech et al., 2011).

The neurons that form the human cerebral cortex are organised into a complex network of local circuits and long-range fibre pathways, facilitating the interaction between specialised brain systems (Hagmann et al., 2008). The PCC is considered a cortical hub,

based on the extensive connections to other brain regions (Hagmann et al., 2008). Investigations have sought to unveil the topology of cortical connectivity and the role of such hubs, in doing so they have observed a consistent and pervasive pattern of activity differing over conditions of rest and cognitive load (Hagmann et al., 2008). Along with the PCC, the ventromedial prefrontal cortex, lateral inferior parietal lobes and medial temporal structures (Raichle et al., 2001) have all been shown to be more active during rest than during cognitively demanding tasks (Leech, Braga & Sharp, 2012; Raichle et al., 2001; Shulman et al., 1997). The dynamically coupled activity of these regions is known collectively as the default mode network (DMN) (Raichle et al., 2001). The PCC is a main node in this network has become its dominant functional characterisation (Greicious et al., 2009; Margulies et al., 2009; Leech et al., 2011). Collectively the DMN is thought to be responsible for emotional processing, memory recall of prior experiences and self-referential mental activity (Raichle, 2015).

The PCC and wider DMN have been shown to display abnormalities in their typical functioning, metabolism, and structure in neurodegenerative, neurological, and psychiatric disorders (Buckner, Andrews-Hanna & Schacter, 2008; Leech & Sharp, 2014; Zhang & Raichle, 2010). The process of healthy aging sees a loss in the connectivity of major DMN nodes, that correlates with age related cognitive impairment (Andrews-Hanna et al., 2007). Furthermore, the normally tightly coupled deactivation off the PCC and other DMN nodes with increasing cognitive load becomes increasingly inefficient (Prakash et al., 2012). It is suggested the disruption in function is reflective of underlying structural abnormalities in white mater connectivity (Leech & Sharp, 2014). The PCC has been shown to be vulnerable to neurodegenerative disease, with hypometabolism of this region being an early sign of Alzheimer's disease (Buckner et al., 2008; Johnson et al., 1998). Metabolic disfunction is also observed in wider PCC connected areas, such as the medial temporal lobe, reflective of a disintegration of the PCCs functional connectivity (Johnson et al., 1998). It has been observed that patterns of atrophy in neurodegenerative disease mirror those connectivity networks, such as the DMN (Seeley et al., 2009). The cause of the early involvement of the PCC and other brain network hubs in neurodegeneration is not known but it may be due to their enhanced metabolic activity predisposing them to the pathological cascades that underlie neurodegenerative disease (Buckner et al., 2009). Therefore, research focusing on the function of the PCC and its metabolism is vital in understanding the topology of this unusual region and could provide insight to its vulnerability to disfunction in diseased states.

1.1.6 Neurovascular uncoupling and reversal

For clarity throughout the thesis, we will distinguish between the states of neurovascular uncoupling and reversed neurovascular coupling. As previous authors have defined it, a reversal in neurovascular coupling is when neural activity that traditionally stimulates a local vasodilatory response to meet the enhanced metabolic needs, is flipped with the activity instead stimulating a vasoconstrictive response and a local reduction in CBF (Kozberg et al., 2013; Rossetti et al., 2020), in functional MRI this would reverse a once positive BOLD response to a negative one, and vice-versa, a once negative response to a positive one. Uncoupling is a state that would result from a disruption of the normal signalling mechanisms that stimulate a propagating vasodilatory response to increase local CBF to meet rising metabolic demand. This would mean local neural activity and enhanced metabolic demands would not be met with an increase in cerebral blood flow or, an insufficient increase (insufficient hyperemia) (Kozberg & Hillman, 2016). If neural activity were to persist in the presence of an uncoupling, you would predict the presence of a negative BOLD signal (Kozberg & Hillman, 2016).

1.2 Thesis Aims, research questions and methodology

This thesis will investigate the human cerebrovascular response to acute periods of hypoxia and examine the relationship between regional vascular and metabolic coupling during this same condition. In completing a series of investigations, we hope to address the open question of whether or not acute hypoxia reverses neurovascular coupling within specific regions of the brain.

1.2.1 Outline of thesis experiments

The first objective in this thesis was to replicate the findings of two previous studies that demonstrate exposure to acute poikilocapnic hypoxia does not result in uniform changes in regional cerebral blood flow across the brain. Specifically, whether posterior regions of the brain known to constitute major nodes of the default mode network, namely the posterior cingulate cortex and angular gyri, display reduced perfusion in response to hypoxia.

The second objective of this thesis was to utilise functional magnetic resonance spectroscopy as a non-haemodynamic dependant measure of task based neural activity within the PCC to reveal if hypoxia reverses neurovascular coupling within this region.

The third objective was to separate the effect of hypoxaemia during poikilocapnic hypoxia from the concomitant state of hypocapnia to answer whether the heterogenous

changes in regional cerebral blood flow are reflective of regional sensitivities to either vascular active state.

The fourth and final objective was to use edited magnetic resonance spectroscopy to allow the acquisition of a full metabolic profile within the PCC to determine whether or not hypoxia results in a change in regional inhibitory tone.

From the studies we have conducted we should be able to ascertain whether changes we have seen in regional cerebral blood flow are the result of metabolic, functional or physiological (vascular response to blood gas changes) effectors during environmental hypoxia.

1.3 Dissemination of research findings

Chapter 2 of this thesis has been published within a peer reviewed journal, referenced below.

Rogan, M., Friend, A. T., Rossetti, G. M., Edden, R., Mikkelsen, M., Oliver, S. J., Macdonald, J. H., & Mullins, P. G. (2022). Hypoxia alters posterior cingulate cortex metabolism during a memory task: a ^{1}H fMRS study. *Neuroimage*, *260*, 119397. https://doi.org/10.1016/j.neuroimage.2022.119397

The data and findings contained within this thesis have been presented at the following academic conferences and symposiums:

Rogan, M., Friend, A. T., Rossetti, G. M., Edden, R., Mikkelsen, M., Oliver, S. J., Macdonald, J. H., & Mullins, P. G. (2021, January). *Hypoxia alters posterior cingulate cortex metabolism during a memory task: a ^{1}H fMRS study*. Academic poster presented at GABA Gabber Symposium, online meeting.

Rogan, M., Friend, A. T., Rossetti, G. M., Edden, R., Mikkelsen, M., Oliver, S. J., Macdonald, J. H., & Mullins, P. G. (2020, October). *Hypoxia alters posterior cingulate cortex metabolism during a memory task: a ^{1}H fMRS study*. Academic poster presented at European Society for Magnetic Resonance in Medicine and Biology (ESMRMB) , online meeting.

Rogan, M., Friend, A. T., Rossetti, G. M., Edden, R., Mikkelsen, M., Oliver, S. J., Macdonald, J. H., & Mullins, P. G. (2021, May). *Hypoxia alters posterior cingulate cortex metabolism during a memory task: a ^{1}H fMRS study.* Oral presentation of work at the Imaging Cerebral Physiology Network (ICP Network): ICP highlights from ISMRM.

Rogan, M., Friend, A. T., Rossetti, G. M., Edden, R., Mikkelsen, M., Oliver, S. J., Macdonald, J. H., & Mullins, P. G. (2021, May). *Hypoxia alters posterior*

cingulate cortex metabolism during a memory task: a ^{1}H fMRS study. Academic poster presented at the International Society for Magnetic Resonance in Medicine (ISMRM): Annual Meeting and Exhibition, online meeting.

Rogan, M., Friend, A. T., Rossetti, G. M., Oliver, S. J., Macdonald, J. H., & Mullins, P. G. (2020, February). *Regional Cerebral Blood Flow-Metabolic Uncoupling during Acute Hypoxia in Humans: A ^{1}H Magnetic Resonance Spectroscopy & Arterial Spin Labelling study*. Oral presentation at the collage of Human Sciences PhD conference, Prifysgol Bangor University, Wales, UK.

Rogan, M., Friend, A. T., Rossetti, G. M., Oliver, S. J., Macdonald, J. H., & Mullins, P. G. (2019, November). *Regional Cerebral Blood Flow-Metabolic Uncoupling during Acute Hypoxia in Humans: A ^{1}H Magnetic Resonance Spectroscopy & Arterial Spin Labelling study*. Academic poster presentation at the British Mountain Medicine Society Science Day, Bamford, England, UK.

Rogan, M., Friend, A. T., Rossetti, G. M., Oliver, S. J., Macdonald, J. H., & Mullins, P. G. (2019, September). *Human cerebral blood flow-metabolic uncoupling during acute hypoxia: A ^{1}H Magnetic Resonance Spectroscopy & Arterial Spin Labelling study*. Poster presentation at the British & Irish Chapter ISMRM, Sheffield, England, UK.

Rogan, M., Friend, A. T., Rossetti, G. M., Oliver, S. J., Macdonald, J. H., & Mullins, P. G. (2019, September*). Human cerebral blood flow-metabolic uncoupling during acute hypoxia: A ^{1}H Magnetic Resonance Spectroscopy & Arterial Spin Labelling study*. Poster presentation at the conference of Extreme Environmental Physiology: Life at the limits, Portsmouth, England, UK.

Chapter 2

Hypoxia alters posterior cingulate cortex metabolism during a memory task: a ^{1}H fMRS study

Rogan, M., Friend, A. T., Rossetti, G. M., Edden, R., Mikkelsen, M., Oliver, S. J., ... & Mullins, P. G. (2022). Hypoxia alters posterior cingulate cortex metabolism during a memory task: a 1H fMRS study. *Neuroimage*, *260*, 119397. Doi: https://doi.org/10.1016/j.neuroimage.2022.119397

Chapter 3

Multimodal Imaging of Regional Cerebral pH and Perfusion in Response to Ventilatory Challenges

Abstract

Upon exposure to hypoxia, the hypoxic ventilatory response increases the breathing rate in attempt to combat arterial oxygen desaturation. Consequently, there is also a fall in the concentration of arterial carbon dioxide, creating a state of hypocapnia. The result is an environment where two opposing vasoactive chemostimuli co-exist, hypoxaemia that promotes vasodilation and hypocapnia that drives vasoconstriction.

Inevitably, the drive for vasodilation succeeds, leading to the well-established observation of increased global cerebral blood flow in response to hypoxia. However, regionally this increase is not uniform, regions including the posterior cingulate and angular gyri have displayed a reduction in perfusion whilst it is enhanced in neighbouring and wider cortical areas. Without an investigation of the regional effect of this state of hypocapnia, or more specifically the regional tissue alkalosis it can induce, it is unknown if the observed heterogeneity in regional cerebral blood flow is in fact reflective or a regional susceptibility to this vasoconstrictive stimulus.

This study aimed to understand the contribution of hypocapnia as a result of hypoxia induced hyperventilation, to the observed reduction in regional perfusion, particularly within the posterior nodes of the default mode network. We used Amide Proton Transfer Imaging, that is sensitive to changes in tissue pH and Arterial Spin Labelling sensitive to changes in regional perfusion.

We revealed that APT can in fact detect changes in tissue pH as a result of hyperventilation induced hypocapnia. Interestingly, despite the posterior cingulate showing reduced perfusion during hypoxia, this is in the absence of a change in tissue pH within that region. Therefore, regional reductions in perfusion during hypoxia within this region are not reflective of regional vasoconstriction as a result of regional tissue alkalosis but instead likely reflective of a neural activity or metabolic change.

Key words: Hypoxia, hypocapnia, Amide Proton Transfer Imaging

3.1 Introduction

Upon exposure to acute hypoxia, reductions in PaO_2 stimulate peripheral chemoreceptors triggering a plethora of physiological responses with the aim of maintaining cerebral/tissue oxygen delivery (CDO_2). One such response is an enhancement in ventilatory drive, termed the hypoxic ventilatory response (HVR). However, the enhancement in alveolar ventilation also results in a reduction of $PaCO_2$, leading to a state of hypocapnia and respiratory alkalosis.

Over time, the alkalosis stimulates a compensatory renal metabolic acidosis, returning pH towards normal within hours to days of exposure to hypoxia. However, individuals acutely exposed to hypoxic environment or hyperventilating in a normoxic environment will develop respiratory alkalosis with arterial pH reaching as high as 7.7 and $PaCO_2$ falling as low as 10 mmHg (from an average resting 40 mmHg) (Grocott et al., 2009; Swenson, 2016). Although the degree of alkalaemia will be dependent on the intensity of hyperventilation, in previous investigations after two hours of poikilocapnic hypoxia (fraction of inspired oxygen; F_IO_2 =0.120), there was on average a 4 (Rossetti et al., 2020) and 5 mmHg reduction (Lawley et al., 2017) in end tidal carbon dioxide ($P_{ET}CO_2$), respectively. There was no measurement of cerebral or systemic pH in these studies. However, acutely we would expect cerebral and systemic pH to vary with changing $PaCO_2$.

Our group has demonstrated regional reductions in resting posterior cingulate perfusion (with some extension to wider posterior regions) after 2.5 hours of poikilocapnic hypoxia. Given that regional cerebral blood flow delivery is coupled to metabolic demand (Raichle et al., 2001), this observation was considered to be the result of a regional reduction or suppression of neural activity and metabolic turnover during hypoxia (Lawley et al., 2017). However, vascular constriction not mediated by neurovascular coupling but instead by hypocapnia, could also be an explanation for this observation given the mild state of hypocapnia was present. Previously, regional variations in the hypocapnic-induced vasoconstriction have been observed, although not localised specifically to the PCC (Ito *et al.* 2000; Schlünzen et al., 2010). However, it must also be noted that Rossetti et al. (2020) found the reductions in PCC perfusion during hypoxia tended to correlate with the degree of hypoxaemia, not hypocapnia. Despite this, Rossetti et al. (2020) was unable to independently assess the effect of either hypoxaemia or hypocapnia, the origins of this vascular phenomenon during poikilocapnic hypoxia remains unknown. To determine the effect of hypocapnia an isocapanic hypoxic stimulus allowing isolation of hypoxaemia or alternatively delivery of hypocapnic stimulus alone, would be required.

Respiratory alkalosis during hypoxia has been implicated in mediating an increase in global $CMRO_2$ through the blunting adenosine generation which mediates neural excitability (Wang et al., 2015; Vestergaard et al., 2016). Supporting this observation, administration of a low dose carbonic anhydrase inhibitor that elevates tissue CO_2 content, reducing tissue pH was found to mitigate the hypoxia-induced increase in $CMRO_2$ (Wang et al., 2015). Using magnetic resonance spectroscopy Vestergaard et al. (2016) demonstrated an increase in occipital lobe glutamate concentrations accompanying increases in $CMRO_2$ after 1 hour of 10% O_2 poikilocapnic hypoxia. They concluded this to reflect enhanced neural excitability because of hypocapnia (Vestergaard et al., 2016). However, on repeat of this investigation with a matched hypoxic stimulus, the changes in glutamate were not replicated (Vestergaard et al., 2017), with the authors suggesting a more homogenous HVR, reducing variability in the degree of hypocapnia and respiratory alkalosis across their participants. Furthermore, with a more moderate hypoxic stimulus, 12% O_2, and a longer exposure (2.5 hours) there was no alteration in metabolites suggestive of a change in resting neural activity within the PCC (findings in chapter 2). Although these investigations have varied in the intensity and duration of their hypoxic stimulus, all have failed to separately investigate the hypocapnic and hypoxaemic contributions to poikilocapnic hypoxia with the tissue and blood gas environment being dependant on each participant's HVR. Furthermore, the resolution of each investigation has either been limited to a specific brain region or a less sensitive global measure that would fail to detect regional variations.

In-vitro measurements of cerebral tissue pH have been challenging within the field of MRI. Phosphorus (^{31}P) spectroscopy does provide a reliable measurement of pH within the brain but this technique lacks spatial resolution and requires specialist MR-equipment (Zhou, 2003). However, chemical exchange saturation transfer (CEST) imaging allows for the indirect detection and measurement of low-concentration solutes, molecules or the microenvironmental conditions within the human brain, that previously would have only been imaged effectively using exogenous contrast agents. When you use a frequency specific saturation pulse that is different to the frequency of bulk water, the saturated protons at that given frequency will exchange with unsaturated bulk water protons (Van Zijil & Yadav, 2011). This exchangeability of the protons results in the water signal becoming attenuated. Given the volume of the water pool within human tissue compared to all other solutes, provided the solute has a fast enough exchange rate whilst exposing it to a continuous RF-pulse, the saturation-transfer effect between the solute and water will be amplified, becoming visible on the water signal (Van Zijil & Yadav, 2011). This chemical exchange saturation

transfer effect is dependent on several factors, including, concentration, temperature and pH (Anemone et al., 2019). At lower pH levels, exchange rates are slower as a result of base-catalysed proton exchange (Ward & Balaban, 2000). Endogenous amide protons found within mobile proteins and peptides within the brain have demonstrated pH weighting when imaging them using the CEST contrast (Anemone et al., 2019). With falling pH reducing the exchange rate and producing a reduction in the CEST effect has been successfully demonstrated using amide proton transfer imaging in models of stroke (Zhou et al., 2003). In animal models of ischaemia, a drop in the APT weighted signal follows the hypoxic insult, in the absence of change in protein concentration and temperature, this is suggested to reflect pH reduction (acidosis). Interestingly, imaging throughout and in hours after reperfusion, the APT weighted signal can be seen to return to control levels, and exceed them, believed to reflect the rebound alkalosis after ischaemic injury (Zheng & Wang, 2017).

This study has attempted to separate and understand the contributions of hypoxaemia and hypocapnia to the observed cerebrovascular and metabolic alterations that accompany poikilocapnic hypoxia. To do this, the present study has utilised a repeated measures design, starting with a resting normoxic control, where participants were instructed to stare at a central fixation cross for each scan. Participants were then asked to voluntarily increase their breathing rate (hyperventilate) to the beat of an auditory metronome to produce a mild reduction in $P_{ET}CO_2$. The goal of this is to replicate the hypocapnic stimulus experienced by participants during poikilocapnic hypoxia, without a change in oxygen saturations. Finally, participants were exposed to a moderate 12% O_2 hypoxic stimulus for 1 hour, during which we would expect participants to experience a mild state of hypocapnia as a result of hypoxia induced hyperventilation.

By subtracting the repeated measures (amide proton transfer maps, arterial spin labelling perfusion maps) in the poikilocapnic hypoxia, voluntary hyperventilation and control (normal breathing) conditions we have identified the neurovascular and metabolic effect of poikilocapnic hypoxia, then isolate the contributions of hypocapnia and hypoxaemia to such effects.

3.2 Methods

3.2.1 Participants

Thirteen healthy adults (5 females) were recruited into the study (mean ± SD); height, 174 ± 6 cm; body mass, 70 ± 10 kg). Participants had not traveled to altitude (> 1500 m) in the preceding six months and had no medical contraindications. Female participants were studied during the early follicular phase of their cycle, or the placebo phase of oral contraceptives. All participants provided written informed consent. Ethical approval was granted by the Ethics Committee of the School of Psychology at Bangor University and carried out in accordance with the WMA Declaration of Helsinki. All scanning procedures were scrutinized and approved by the Bangor Imaging Unit steering committee (Ethical approval number 2019-16489).

3.2.2 Study Design

The study followed a repeated-measures design. All participants were first scanned under the normoxic condition, (fraction of inspired oxygen; $F_IO_2 = 0.209$). At the end of this period they completed a 12-minute hyperventilation challenge. The first 2 minutes of the challenge the participant increased their rate of breathing in time with a auditory metronome, they then maintained this for a further 10 minutes. When the reduction in end-tidal CO_2 appeared to plateau (after the first two minutes), a 5-minute APT scan and 5-minute ASL scan were acquired during the remaining 10 minutes. The same scan parameters as the normoxic session were employed. Participants were then removed from the scanner and were exposed to the hypoxic condition ($F_IO_2 = 0.120$) for one hour at rest. This was achieved as explained in subsection 3.2.3 below. Participants then returned to the scanner, still exposed to the same hypoxic environment and the scans collected during the first normoxic session were repeated. Whilst hypoxic, physiological data were collected at 15-minute intervals. During the MRI sessions, T_1-weighted structural images and arterial spin labelling measures of resting perfusion were collected in each condition. Magnetic Resonance Spectroscopy was also conducted in both conditions whilst the participant was at rest, the results of these investigations are displayed and interpreted later in this chapter. See appendices H for visual representation of procedure.

3.2.3 Experimental protocol

All procedures were performed within 50 m of sea level. The hypoxic environment was simulated by filling 1000 L Douglas bag containing $F_IO_2 = 0.209$ or $F_IO_2 = 0.120$ (dependent on session condition). Participants wore a leak-free face mask connected to a two-

way Hans Rudolph valve, preventing rebreathing of air. The inspiratory port was connected to the Douglas bag via Falconia tubing.

3.2.4 Physiological monitoring

Physiological monitoring was conducted throughout the experiment. Expired carbon dioxide (CO_2) was sampled from the face mask for a five-minute interval during the acquisition of the arterial spin labelling scans in both conditions. CO_2 concentrations were estimated using a calibrated fast responding gas analyzer (GC-0017 (0-20%) SprintIR CO_2 Sensor; GSS, Cumbernauld, UK), and recorded using CO_2 logging software (GasLab; CO_2Meter, Inc.; Florida, USA). The partial pressure of end-tidal CO_2 ($P_{ET}CO_2$) was calculated from the recorded CO_2 trace using peak detection software within the pracma package (Version 2.3.3, Borchers, 2018) in RStudio (Version 1.3.1073; RStudio Team, 2020). Heart rate, oxygen saturation (S_pO_2) and blood pressure were measured on one occasion just prior to entering the scanner for the normoxic condition. When participants were exposed to the 1 hour of hypoxia before getting into the MRI scanner, the measurements were taken at 15-minute intervals up until the point the entered the scanner.

Exposing humans to an acute hypoxic environment can be accompanied by the development of acute mountain sickness (AMS) symptoms. To track the development of this condition participants were administered the Lake Louise Questionnaire (LLQ) (Roach et al., 2018) at thirty-minute intervals throughout the experimental protocol. See appendices J for example LLQ. Clinical AMS was defined as scoring ≥ 3 on the LLQ with the presence of headache and at least one other symptom. The presence of clinical AMS during the protocol was an exclusion criterion.

3.2.5 MRI scanning

Anatomical imaging

All MRI sequences were conducted on a 3T Philips Ingenia Elition X (model R.5.6.1) MRI scanner (Philips Healthcare) using a 32-channel head coil. Anatomical image scans were acquired at the beginning of each scan protocol, immediately after a brief survey scan in both the normoxia and hypoxia experimental sessions. High resolution T_1-weighted images were acquired as a five-echo MP-RAGE sequence (TE = 3.5, 10.5, 20.5, 30.5, 40.5 ms; TR = 45 ms, TI = 1150 ms; 3D acquisition; field-of-view = 225 mm × 225 mm × 175 mm; voxel dimensions = 1 × 1 × 1 mm^3, SENSE = 2). The five echoes were then averaged to produce a

single image used for registration of the arterial spin labelling scans, locating the HERMES MRS acquisition voxel and subsequent tissue segmentation.

Arterial Spin Labelling

To measure whole brain resting perfusion, ASL images were acquired after the structural imaging and before the acquisition of the MRS data. ASL images were acquired using the standard 3D pseudo continuous arterial spin labelling package provided with the scanner. Each scan consisted of 14 slices with a 224 X 224 mm^2 field of view (FOV) and 2 X 2 X 6 mm^3 in plane resolution. All slices were aligned perpendicular to the Z-axis of the scanner. Images were acquired as 16 matched tag and one control images with a TR = 4 s, TE = 12 ms and total scan time of 4 min 42 s. In line with the consensus recommendations, the labelling duration and post labelling delay were 1800 ms long and spectral presaturation with inversion recovery (SPIR) fat suppression was used (Alsop et al., 2015).

Image analysis was performed using the FMRIB Software Library (FSL) v6.0.5.2 MP-RAGE images were brain extracted using BET (Smith, 2002) then segmented using FAST (Zhang, Brady & Smith, 2001). ASL data were analysed using BASIL (Chappell et al., 2008). As ASL signal is dependent on blood T_1, and as blood T_1 values are dependent on haematocrit and blood oxygenation we corrected the blood T_1 estimates used in BASIL via the model of Hales et al. (2016) for each participant using their haematocrit and SpO_2 values for each imaging session. Automatic estimation of bolus duration was applied. The CBF maps produced by BASIL were registered to the T_1-weighted structural images, smoothed with a 4-mm Gaussian kernel, masked with the grey matter image from the T_1 segmentation, and registered to the "Montreal Neurological Institute (MNI) 2 mm" T_1-weighted average image for group comparison, using the FMRIB Linear Image Registration Tool (FLIRT) (Jenkinson & Smith, 2001; Jenkinson, Bannister, Brady & Smith, 2002).

Amide Proton Transfer Imaging

We used the APT Imaging protocol that is provided by Phillips Medical (Van De Ven & Keupp, 2018).

APT images were acquired using a 3D spin echo sequence, over 14 slices with reconstructed voxel size of 2X2X6, TR = 5864 ms, TE = 8.3 ms, SPIR fat suppression was on. The RF saturation pulse train B_1 = 2 μT, T_{sat} = 2 s (saturation duration).

Native space APT images were registered to a T1 structural image and then transformed into "Montreal Neurological Institute (MNI) 2 mm" T_1-weighted average space

for group comparison using the FMRIB Linear Image Registration Tool (FLIRT) (Jenkinson & Smith, 2001; Jenkinson, Bannister, Brady & Smith, 2002).

The amide proton transfer images in the present study were created using the analysis pipeline detailed within the Philips Medical 3D APT whitepaper (Van De Ven & Keupp, 2018). In brief, to generate reliable APTw images, the magnetisation transfer ratio asymmetry (MTR_{asym}) is assessed. This involves the acquisition of a z-spectrum, formed of the changes in the bulk water resonance as a function of the RF-pulse at differing resonances offset from the water resonance (Anemone et al., 2019; Van De Ven & Keupp, 2018). Asymmetry is evaluated by subtracting the positive side ($S_{\Delta\omega}$) from the negative ($S_{-\Delta\omega}$), then dividing or normalising by an unsaturated image (S_0), see equation 1 (Van De Ven & Keupp, 2018). Finally, APTw% is the difference between the z-spectrum at +/- 3.5ppm normalised to an unsaturated image, see equation 2 (Van De Ven & Keupp, 2018). This analysis is performed on a voxel-by-voxel level (Van De Ven & Keupp, 2018). Using a field map (B_0), the z spectrum is aligned to ensure the 0 point is at the maximum direct water saturation, thus accounting for local field inhomogeneity (Van De Ven & Keupp, 2018).

Equation 1. Calculation of magnetisation transfer ratio asymmetry percentage.

$$MTR_{asym}\ (\%) = (S_{-\Delta\omega} - S_{\Delta\omega})/S_0$$

Equation 2. Calculation of amide proton transfer weighting percentage.

$$APTw\% = MTR_{asym}\ [\Delta\omega + 3.5ppm](\%)$$

3.2.6 Statistical comparisons

Comparison of physiological data between conditions

A paired samples T-test was used to compare heart rate and arterial oxygen saturation, this was calculated using Jamovi statistical software package (R Core Team, 2019; The Jamovi Project, 2020). To compare the change in $P_{ET}CO_2$ across the three conditions, namely normoxia, hypoxia and hyperventilation, a 1X3 repeated measures ANOVA was calculated using Jamovi software package (Lenth, 2018; R Core Team, 2019; Singmann, 2018; The Jamovi Project, 2020).

Perfusion comparisons between conditions

Arterial spin labelling maps of perfusion were quantified for each condition, namely, normoxia, hypoxia and hypocapnia. Each of these conditions were compared using a one sample t-test in Randomise (cluster mass FWE correction at $p < 0.05$).

Amide Proton Transfer comparison between conditions

Amide proton transfer maps were quantified for each condition, namely, normoxia, hypoxia and hypocapnia. Each of these conditions were compared using a one sample t-test in Randomise (cluster mass FWE correction at $p < 0.05$).

3.3 Results

3.3.1 Physiology

Compared to normoxia, 1 h of poikilocapnic hypoxia increased heart rate by 11 bpm (95% CI: [17, 4]; P=0.003) and reduced peripheral arterial oxygen saturation by 13% (95%CI: [10, 15]; P<0.001).

$P_{ET}CO_2$ was measured during the acquisition of the APT scans in each of the three conditions. In normoxia, the average (M±SD) across participants was 42±5 mmHg. After 1 hour of poikilocapnic hypoxia this slightly fell to 37±15 mmHg and during the hyperventilation challenge, it fell to its lowest at 33±7 mmHg. Statistical comparison of the change in $P_{ET}CO_2$ across these three conditions reveal a trending to significant main effect of condition (F(2,12)=3.09,P =.064). Post hoc analysis show that this trending significant result is being driven by the change on CO_2 between normoxia and hypocapnia (P=.061).

See appendices K for table of physiology results.

3.3.2 Arterial Spin Labelling

Comparison of regional cerebral perfusion across all participants between the normoxic and hypocapnic condition, revealed uniform reductions in perfusion across the cortical grey matter during hypocapnia compared to that in normoxia (see figure 3.1). No region within the brain displayed any significant clusters of increased perfusion during hypocapnia compared to normoxia (see figure 3.1).

In accordance with the comparison made in chapter 2, we also compared regional cerebral perfusion during hypoxia to that in normoxia. We revealed clusters of significantly reduced perfusion during hypoxia compared to normoxia that encompassed the posterior cingulate cortex, bilateral angular gyri and temporal cortices. There were some remote clusters within the outer frontal cortex (see figure 3.2). Interestingly, few regions' studied

showed any significant clusters enhanced perfusion during hypoxia compared to normoxia with only a few remote and isolated clusters (see figure 3.2).

Our final set of comparisons were between perfusion during hypoxia and perfusion during the hypocapnia condition. There were clusters indicating perfusion during hypocapnia was significantly increased compared to hypoxia (see figure 3.3). Significant clusters of increased perfusion during hypoxia compared hypocapnia were identified across the brain (see figure 3.3). However, the coverage of these clusters was less extensive than those increases observed between normoxia and hypocapnia, captured in figure 3.1. This is indicative of the fact that perfusion in some regions is lower during hypoxia than normoxia.

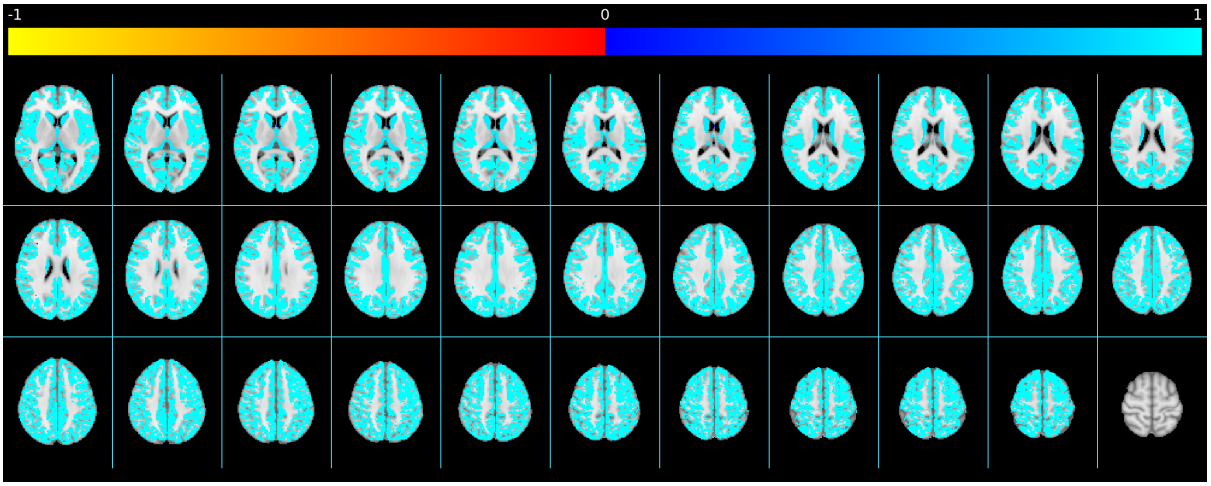

Figure 3.1. Blue to light blue represents clusters of significantly reduced perfusion between the normoxia and hypocapnia conditions. Red to yellow represents clusters of significantly increased perfusion between normoxia and hypocapnia. Clusters were calculated using the FSL tool RANDOMISE with cluster-based thresholding and family-wise error correction (FWE) correction set at $p < 0.05$.

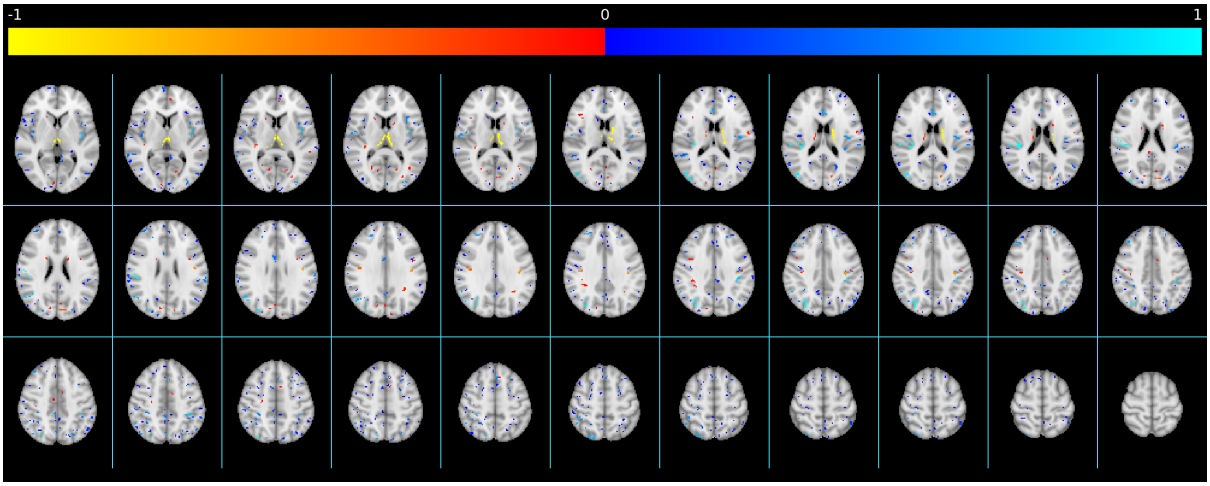

Figure 3.2. Blue to light blue represents clusters of significantly reduced perfusion between the normoxia and hypoxia conditions. Red to yellow represents clusters of significantly increased perfusion between normoxia and hypoxia. Clusters were calculated using the FSL tool RANDOMISE with cluster-based thresholding and FWE correction set at $p < 0.05$.

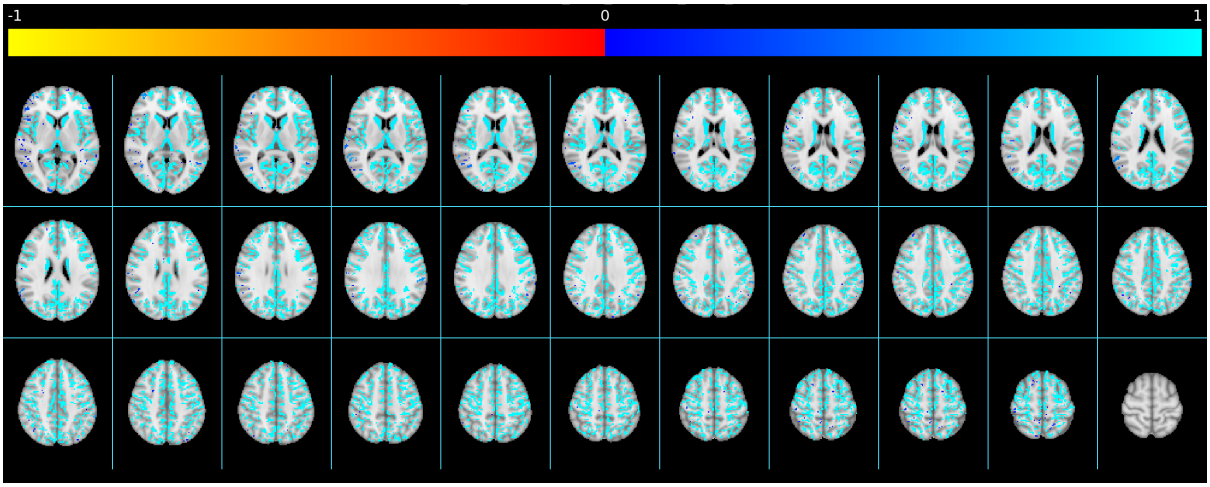

Figure 3.3. Blue to light blue represents clusters of significantly reduced perfusion between the hypoxia and hypocapnia conditions. Red to yellow represents clusters of significantly increased perfusion between hypoxia and hypocapnia. Clusters were calculated using the FSL tool RANDOMISE with cluster-based thresholding and few correction set at $p < 0.05$.

3.3.3 Amide Proton Transfer Imaging

The same condition contrasts for the Arterial Spin Labelling maps were repeated for the Amide Proton Transfer weighted maps.

The APT weighted signal was compared between normoxia and hypocapnia. Significant clusters indicating increased APT signal intensity in the normoxic condition compared to the hypocapnic conditions were found in the lower areas of the brain around the

ventricles and lower left occipital cortex (see figure 3.4). There were also some isolated and restricted clusters within the left superior occipital cortex and bilateral superior frontal gyri. However, reversing the contrast comparison and revealing the regions that displayed greater APT weighted signal intensities in hypocapnic compared to normoxic condition revealed more extensive cluster coverage (see figure 3.4). Significant increases were located within the bilateral insulas, extending towards in inferior frontal gyrus and pole. Going superior, the clusters also extended to the bilateral parietal cortices and angular gyri. Significant clusters were also identified within the precuneous and posterior cingulate cortex, bilateral lateral occipital cortices and supramarginal gyri. Going more superior within the cortex the clusters become more fragmented but still appear within postcentral gyri and superior parietal lobule.

The APT weighted signal was also compared between normoxia and hypoxia. Significant clusters indicating increased APT-weighted signal in normoxia were located within the lower part of the brain and are found within the right front pole region, precentral gyrus and central opercular cortex (See figure 3.5). In the more superior parts of the brain, clusters are seen within the region of the right postcentral gyrus and left occipital lobe, post central and supramarginal gyri. Significant clusters of increased APT weighted signal during hypoxia compared to normoxia in lower regions of the brain were located within the left frontal pole and around the right caudate (see figure 3.5). Within figure 3.5 there is a cluster that appears to strike through the white matter of the right hemisphere, we believe this to be an artefact although there is no significant distortion in the images upon inspection. Within the superior parts of the brain, clusters are found within the mid and posterior areas particularly on the right hemisphere with limited clusters within the superior parietal lobule, supramarginal gyrus and precuneous.

The APT weighted signal was also compared between hypocapnia and hypoxia. Significant clusters indicating higher APT-weighted signal in hypocapnia compared to hypoxia were found widespread throughout the bilateral temporal and parietal cortices (see figure 3.6). The distribution is similar but less extensive to that seen in figure 3.4. Clusters were located within the following regions, bilateral central and parietal operculum cortex, precuneous, post central and supramarginal gyrus. In the reverse comparison, showing clusters where the APT-weighted signal is greater in hypoxia than hypocapnia, in the lower regions of the brain there are two isolated clusters in the left hemisphere frontal pole region (see figure 3.6). Ascending within the brain the clusters in the front of the brain continue into the left hemisphere superior frontal gyrus, there are also clusters within the superior occipital cortex.

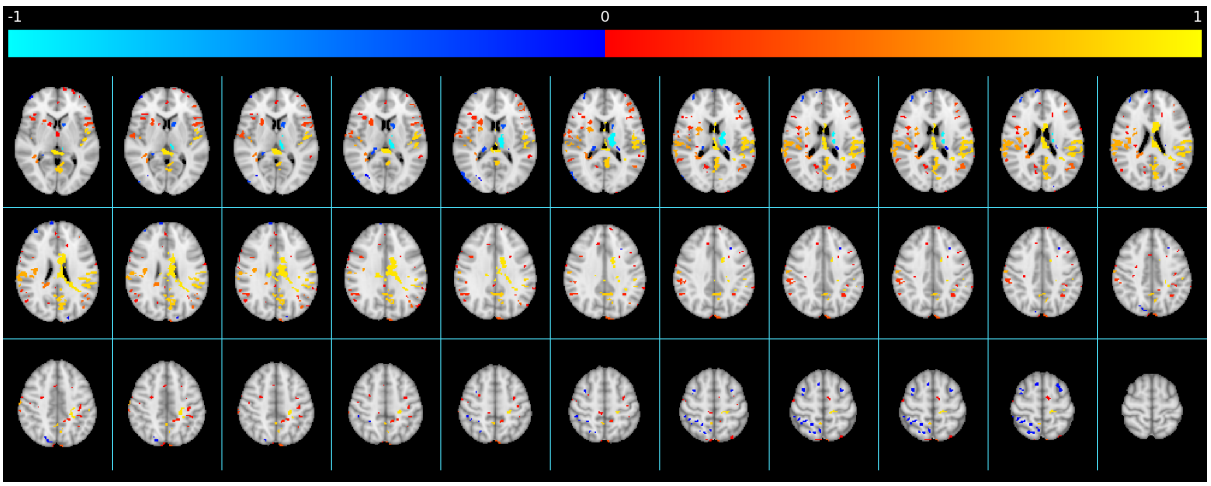

Figure 3.4. Blue to light blue represents clusters of significantly reduced APT signal between the normoxia and hypocapnia conditions. Red to yellow represents clusters of significantly increased APT signal between normoxia and hypocapnia. Clusters were calculated using the FSL tool RANDOMISE with cluster-based thresholding and FWE correction set at $p < 0.05$.

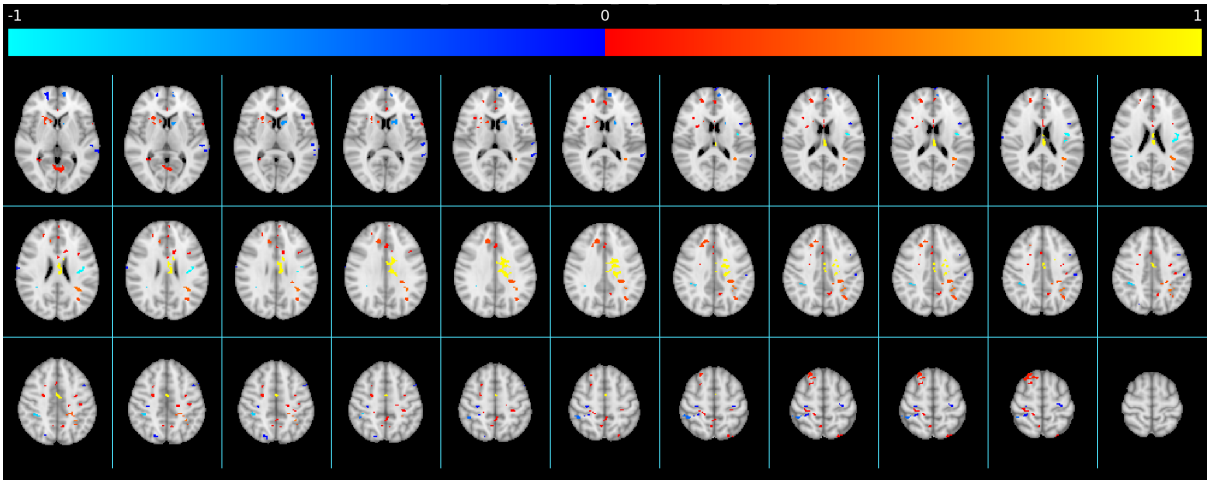

Figure 3.5. Blue to light blue represents clusters of significantly reduced APT signal between the normoxia and hypoxia conditions. Red to yellow represents clusters of significantly increased APT signal between normoxia and hypoxia. Clusters were calculated using the FSL tool RANDOMISE with cluster-based thresholding and few correction set at $p < 0.05$.

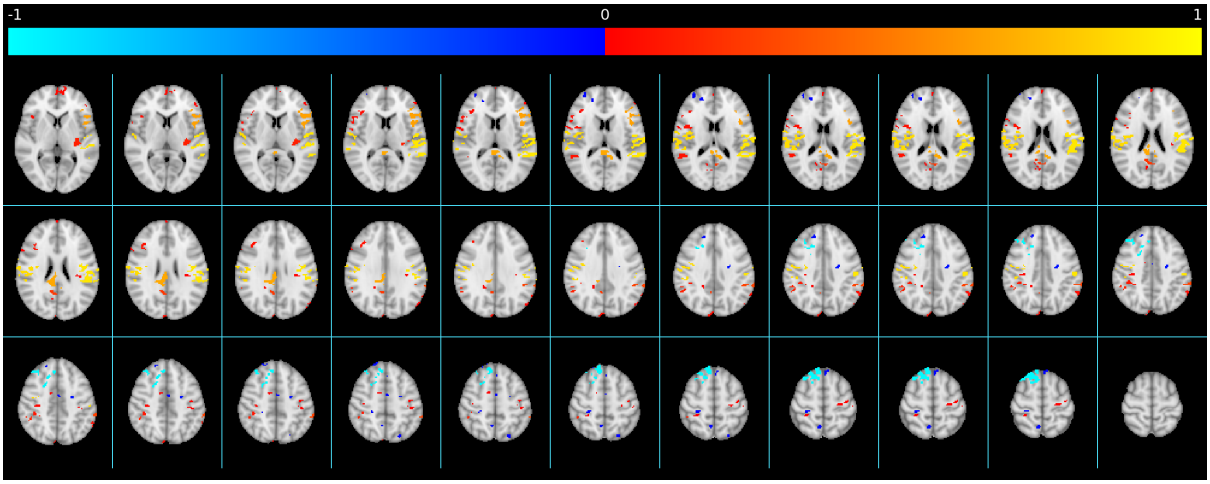

Figure 3.6. Blue to light blue represents clusters of significantly reduced APT signal between the hypoxia and hypocapnia conditions. Red to yellow represents clusters of significantly increased APT signal between hypoxia and hypocapnia. Clusters were calculated using the FSL tool RANDOMISE with cluster-based thresholding and FWE correction set at $p < 0.05$.

3.4 Discussion

In this study we have quantified regional cerebral blood flow using arterial spin labelling and regional tissue pH, inferred from the amide proton transfer weighted signal during normoxia (room air, F_iO_2 .201), poikilocapnic hypoxia (F_iO_2 .102) and hypocapnia, achieved through voluntary hyperventilation breathing normoxic room air. The aim of this investigation was to assess whether heterogenous regional cerebral blood flow changes after 1 hr of poikilocapnic hypoxia could be explained by a regional sensitivity to respiratory alkalosis (increased tissue pH), that ensues during exposure to poikilocapnic hypoxia.

3.4.1 Arterial Spin Labelling Measures of Regional Perfusion

As in previous studies, the present has demonstrated that after a 1-hour exposure to hypoxia, the accompanying changes in regional cerebral blood flow are not homogenous (Lawley et al., 2017; Nöth et al., 2008; Ogoh et al., 2013; Rosetti et al., 2020; Willie et al., 2012). Notably, the posterior portion of the cingulate gyrus and the bilateral insulas display a significant reduction in perfusion during hypoxia compared to normoxia, which replicates the findings of Rossetti et al., (2020). The cause of this reduction in perfusion is still a debate, however, chapter 2 in this thesis has demonstrated that the PCC does not show an alteration in resting glutamatergic signalling, despite a reduction in perfusion. Therefore, this change in perfusion is not coupled to variations excitatory neural activity and its associated metabolic demands. However, in chapter 2 we were unable to obtain a full metabolic profile of the PCC

during hypoxia. Neurochemicals such as GABA and lactate were not reliably quantified which are indicative of neural inhibitory tone and non-oxidative metabolism, respectively. A shift in the balance of oxidative and non-oxidative metabolism and/or suppression of excitatory neural activity and metabolic demand as a defence against hypoxia (Hochachka et al., 1996; Hochachka et al., 1999) are potential explanations for changes in regional CBF which need to be further investigated using edited MRS acquisition schemes.

An explanation for the heterogenous alterations in regional cerebral blood flow during hypoxia could be a regional sensitivity to respiratory alkalosis that occurs during exposure to poikilocapnic hypoxia. Previous work that has focused on measuring blood flow in the large extra-cranial arteries has indicated that hypocapnia, forming as a result of enhanced ventilation during poikilocapnic hypoxia, negates the hypoxia induced increases in the blood flow in the carotid but not vertebral arteries (Ogoh et al., 2013). To further understand if hypocapnia could be contributing to the reduction in regional blood flow seen in our study, we had participants increase their breathing rate for a 10-minute period, inducing hypocapnia and a state of cerebral tissue alkalosis. We have demonstrated that a mild state of hypocapnia induced by enhanced voluntary breathing rate significantly reduced cerebral blood flow across all regions of the brain. This is reflective of the potent vaso-active effects of changes in arterial CO_2 concentration. Reductions in the concentration of arterial and tissue CO_2, which will result in an acute increase in cerebral pH has triggered vasoconstriction, resulting in the global reduction in blood flow we have measured using ASL.

3.4.2 Amide Proton Transfer Imaging

During the hypocapnia condition, the APT signal across large parts of the brain was found to increase, compared to the APT signal in both the normoxia and hypoxia conditions. These differences in APT signal seemed to be somewhat less extensive when comparing hypoxia with hypocapnia, but still present.

The APT signal is known to be weighted by pH. Reductions in the signal are related to tissue acidosis (Anemone et al., 2019; Ward & Balaban, 2000), whereas increases reflect alkalosis (Zheng & Wang, 2017). Given, that participants were in a state of hypocapnia due to increased breathing, we suggest that the increased APT weighted signal indicates a state of regional tissue alkalosis.

Interestingly, unlike the regional CBF during the hypocapnia condition, the increase in the APT signal is not uniform, with some regions displaying an increase, while others remain unchanged. Investigations of regional cerebral pH have found significant variation in

tissue pH across different brain regions (Rijpma et al., 2018; Lyros et al., 2020). The differences in pH were found not to relate to differences in the volume of grey and white matter and instead thought to be reflective of physiological differences and metabolism between regions (Rijpma et al., 2018). Therefore, the heterogeneity in the change in the APT during enhanced respiration could be reflective of the differences in the baseline pH status of different brain regions.

Furthermore, in this study participants were only subject to hyperventilation for around 10 minutes, this was enough to see a significant fall in arterial CO_2 content, which would have resulted in a degree of cerebral tissue alkalosis. However, the degree of tissue alkalosis will be reflective of the specific tissues ability to buffer the change in pH as a result of falling CO_2 concentration (Berg & Meyer, 2008). Within a matter of minutes and lasting to hours, the first line of defence in buffering the alkalosis would be release of intracellular sources of H^+ [hydrogen ions] (Berg & Meyer, 2008; Vepraskas, Troth & Weisgerber, 2023). Renal compensation would occur after prolonged period of alkalosis, towards 24 hours (Carlson & Bruss, 2008). Therefore, we could speculate that the heterogeneity in the change in APT signal could be reflective of differences in the buffering capacity of the underlying tissue regions.

When we compare the APT maps between normoxia and hypoxia, we do not see the same distribution of changes in the signal as we do with the comparison between normoxia and hypocapnia and hypoxia and hypocapnia. This suggests that during hypoxia there is not a regional alteration in tissue alkalosis. If we then consider the matched CBF map comparison, the change in CBF does not appear to be driven by a regional change in pH or, regional alkalosis. This prompts the conclusion that regional alterations in CBF that have been seen in the PCC and bilateral insulas, are not the result of those same regions having enhanced sensitivity to hypoxia induced alkalosis. There is some other mechanism exerting influence over regional CBF during hypoxia.

There are regions of the brain that instead appear to show a reduction in the APT signal during hyperventilation. These appear to be located in the subcortical regions, namely, the palladium, caudate and putamen. The reduction in the signal would suggest that pH in those regions is reducing, resulting from the presence of a mild regional acidosis. This regional acidosis would be the result of an accumulation of CO_2 both intra and extra cellular and/or a build-up of acids that are a by-product of a metabolic process (Rhencrona, 1985).

Subcortical regions have been shown to be protected in comparison to wider cortical areas during other neurovascular challenges, such as exposure to hypoxia (Binks et al., 2008).

This was thought to be reflective of a defence mechanism for those regions that support homeostatic functions (Binks et al., 2008; Noble, Jones & Davis, 1993). Binks et al., 2008 showed the putamen, palladium and caudate among others to have amongst the greatest changes in regional CBF to normocapnic hypoxia. However, replication of this investigation under poikilocapnic hypoxia, where participants were observed to experience a mild state of concomitant hypocapnia, ameliorated the extensive sub-cortical regional CBF enhancement compared to wider cortical regions (Buck et al., 1998). Therefore, subcortical regions do not appear to show any enhanced resistance against the vasoconstrictive effect of hypocapnia.

Our observation of reduced APT signal in these subcortical regions could be reflective of a regional sensitivity to the prevailing state of hyperventilation induced hypocapnia, resulting in a mild state of acidosis. It would be difficult to distinguish if this was being driven by insufficient oxygen delivery, driving up glycolysis and producing metabolic by-products or inefficient CO_2 removal in region with an enhanced metabolic turnover. Few studies have examined the regional effect of hypocapnia on CBF regulation and metabolism. It has been shown that in comparison to frontal, occipital and parietal cortical grey matter, sub cortical regions including the striatum, thalamus and cerebellum displayed smaller changes in BOLD signal amplitude from rest to three minutes of hyperventilation (Posse et al., 1997). They conclude the differences are indicative of regional variability in metabolic activity, vascular regulation and/or capillary density (Posse et al., 1997). This would suggest the subcortical regions are less affected by hyperventilation induced hypocapnia, the opposite to what we have observed. We therefore need to consider inherent issues with our data collection, such as low sample size and the fact we did not employ any strategies to limit head movement during periods of enhanced breathing.

3.4.3 Conclusion

This study investigated whether hypoxia induced reduction in regional cerebral blood flow in PCC could be explained by regional tissue alkalosis caused by hypoxia induced hypocapnia. We demonstrated that voluntary hyperventilation caused a uniform reduction in regional cerebral blood across the brain. Concomitantly, the APT signal across large areas of the brain increases, we believe the increase in this signal reflects increases in regional pH as a result of local tissue alkalosis. During hypoxia, the PCC and bilateral insulas display a reduction in perfusion compared to that seen in normoxia. However, these same regions do not show a significant increase in the APT signal. This allows us to conclude that the hypoxia

induced reduction in region CBF are not the result of hyperventilation induced changes in tissue alkalosis and the subsequent stimulated regional vasoconstriction.

3.5 Author contribution statement.

Matthew Rogan (MR), Prof Paul Mullins (PM), Prof Sam Oliver (SO), Prof Jamie Macdonald (JM).

Project administration (MR, PM), visualisation (MR), conceptualisation (MR, PM, SO, JM), formal analysis (MR), writing of chapter (MR), review of chapter (PM, SO, JM), supervision (PM, SO, JM)

3.6 Acknowledgements

I would like to thank Joseph Smith for assistance with data acquisition, Andrew Fisher for providing MR-technician assistance and Kevin Williams for help with setup and standard protocols for hypoxia.

Chapter 4

Low Concentration Metabolite Dynamics in the Posterior Cingulate Cortex During Hypoxia

Abstract

Exposure to poikilocapnic hypoxia, akin to that encountered at high altitude, has been shown to result in heterogenous changes regional cerebral blood flow. Furthermore, the posterior cingulate cortex (PCC), a region which has shown reduced perfusion during hypoxia, also displays a reversed BOLD response to task when being complete under hypoxic conditions. To further investigate this, the task based neurochemical dynamics were measured and showed that hypoxia negates the task-based increases in glutamate within the PCC. This points towards hypoxia causing a shift towards non-oxidative metabolism and an alteration, rather than reversal, in neurovascular coupling within this region.

To further understand the neurometabolic and vascular phenomenon's within the PCC during exposure to hypoxia, a comprehensive neurochemical profile of it is required. Previous investigations have used Magnetic Resonance Spectroscopy sequences not optimised for the detection of low concentration metabolites. Particularly, the main inhibitory neurotransmitter GABA

This study has used HERCULES, an edited spectroscopic imaging technique, to measure the concentration of low concentration metabolites within the PCC after 1 hour of hypoxia. The concentration of GABA in the PCC was increased by 26% (P=0.005) after 1 hour of hypoxia, the concentration of lactate also increased (P=0.001). Choline (P=0.002), creatine(P=0.007) and myoinositol (P=0.013) were all significantly reduced.

We conclude that hypoxia causes an increase in inhibitory tone within the PCC, limiting excitatory neurotransmission. There is also a shift to non-oxidative metabolism to support the metabolic demands of the region in face of hypoxic stress. The results of the study provide the most comprehensive neurometabolic investigation of the PCC during acute poikilocapnic hypoxia.

Key words: hypoxia, neurovascular coupling, GABA, HERCULES, inhibitory tone.

4.1 Introduction

Upon exposure to hypoxia, global cerebral blood flow (gCBF) increases concomitantly with falling arterial oxygen saturations (Ainslie & Subudhi, 2014). The increase in gCBF is hypothesised to maintain cerebral oxygen delivery and sustain the global cerebral metabolic rate of oxygen ($CMRO_2$) (Ainslie et al., 2014). However, on a regional level, the increases in CBF are not uniform (Rossetti et al. 2020; Lawley et al., 2017; Nöth et al., 2008). Particularly, the posterior cingulate cortex (PCC) has repeatedly displayed reduced perfusion during hypoxia. Given that the delivery of cerebral blood flow is supposedly matched to regional metabolic demand, in a relationship termed neurovascular coupling (Duncombe et al., 2017), this would imply concomitant reductions in CBF and metabolism.

The assumption that increases in global cerebral blood flow sustain cerebral metabolic demand is contradicted by the finding that exposure to moderate hypoxia results in altered cerebral metabolism (cerebral metabolic rate of oxygen) (Jensen et al., 2018; Smith et al., 2013; Vestergaard et al., 2016; Wang et al. 2015). The vast majority of these previous works have largely focused on global measures of metabolism, the fluctuations of which have been attributed to varying degrees of systemic hypocapnia (Smith et al., 2013; Vestergaard & Larson, 2019) that ensues with the hypoxic ventilatory response, rather than hypoxaemia *per se*. Furthermore, most of the work in this field has utilised global measures of metabolism that lack sensitivity to any regional alterations which may be expected given the CBF findings (Rossetti et al. 2020; Lawley et al., 2017; Nöth et al., 2008).

Our group has utilised magnetic resonance spectroscopy and arterial spin labelling to probe regional cerebral blood flow and metabolism during hypoxia. We demonstrated that the posterior cingulate cortex displays a reduction in CBF in the absence of any significant change in metabolism in that same region (findings, chapter 2). This indicates that changes in CBF within the PCC during hypoxia are dissociated from regional metabolic changes. Furthermore, when engaged in a memory recall task that results in increased PCC glutamate levels, exposure to hypoxia negates this glutamatergic response. The absence of a glutamatergic response to task during hypoxia could be explained by two mechanisms: either a hypoxia-induced inhibitory mechanism in the region, or cerebral blood flow-metabolic uncoupling.

Proton MRS allows the detection and measurement of neurochemical concentrations, both when the brain is at rest, and when it is active (Mullins, 2018). This is achieved through the measurement of peak heights in the MR spectrum, and comparison with a reference metabolite, most commonly water. Magnetic Resonance Spectroscopy at 3 T or lower results

in a spectrum where metabolites found in greater abundance will overlap and mask those with a lower concentration and matched resonances on the proton spectrum. This results in a spectrum in which the lower concentration metabolites cannot be reliably resolved. However, knowing the resonant frequency of a low concentration metabolite, and how its spectral pattern may evolve due to j-coupling, it is possible to tailor the MRS acquisition using "editing" pulses to remove the overlapping signals of more abundant, but uncoupled, metabolites. This allows direct resolution and quantification, and can provide a fuller metabolic profile of any region of the cortex to be acquired

In this study we will use an edited MRS acquisition scheme (Oeltzschner et al., 2019) that is optimised for the detection of gamma-aminobutyric acid (GABA), the main inhibitory neurotransmitter of the brain (Rae, 2014). Changes in the concentration of GABA measured using MRS index changes in inhibitory neurotransmission (Takado et al., 2021). We will also use arterial spin labelling to measure tissue perfusion within the PCC after exposure to one hour of hypoxia. This will allow us to assess whether changes in regional cerebral blood flow during hypoxia are reflecting regional changes in neural inhibitory tone. We predict that exposure to one hour of hypoxia will have no effect on the concentration of GABA within the PCC, whilst regional CBF in this area will be reduced. This will indicate that hypoxia results in cerebral-blood flow metabolic uncoupling at a regional level within the PCC.

4.2 Methods

4.2.1 Participants

Thirteen healthy adults (5 females) were recruited into the study (mean ± SD): height, 174 ± 6 cm; body mass, 70 ± 10 kg. Participants had not traveled to altitude (> 1500 m) in the preceding six months and had no medical contraindications. Female participants were studied during the early follicular phase of their cycle, or the placebo phase of oral contraceptives. All participants provided written informed consent. Ethical approval was granted by the Ethics Committee of the School of Psychology at Bangor University, and carried out in accordance with the WMA Declaration of Helsinki. All scanning procedures were scrutinized and approved by the Bangor Imaging Unit steering committee. (Ethical approval number 2019-16489).

4.2.2 Study Design

The study followed a repeated-measures design. All participants were first scanned under normoxic conditions, (fraction of inspired oxygen; $F_IO_2 = 0.209$). They were then removed from the scanner and were exposed to the hypoxic condition ($F_IO_2 = 0.120$) for one hour at rest. They were then placed back into the scanner, still exposed to the same hypoxic environment, and the scans collected during the first normoxic session were repeated. Whilst hypoxic, physiological data were collected at 15-minute intervals. During the MRI sessions, T_1-weighted structural images and arterial spin labelling (ASL) measures of resting perfusion were collected in each condition. Magnetic Resonance Spectroscopy was also conducted in both conditions whilst the participant was at rest.

4.2.3 Experimental protocol

All procedures were performed within 50 m of sea level. The hypoxic environment was simulated by filling 1000 L Douglas bag containing $F_IO_2 = 0.209$ or $F_IO_2 = 0.120$ (dependent on session condition). Participants wore a leak-free face mask connected to a two-way Hans Rudolph valve, preventing rebreathing of air. The inspiratory port was connected to the Douglas bag via Falconia tubing.

4.2.4 Physiological monitoring

Physiological monitoring was conducted throughout the experiment. Expired carbon dioxide (CO_2) was sampled from the face mask for a five-minute interval during the acquisition of the arterial spin labelling scans in both conditions. CO_2 concentrations were estimated using a calibrated fast responding gas analyzer (GC-0017 (0-20%) SprintIR CO_2 Sensor; GSS, Cumbernauld, UK), and recorded using CO_2 logging software (GasLab; CO_2Meter, Inc.; Florida, USA). The partial pressure of end-tidal CO_2 ($P_{ET}CO_2$) was calculated from the recorded CO_2 trace using peak detection software within the pracma package (Version 2.3.3, Borchers, 2018) in RStudio (Version 1.3.1073; RStudio Team, 2020). Heart rate, oxygen saturation (S_pO_2) and blood pressure were measured once prior to entering the scanner for the normoxic condition. They were then measured at fifteen-minute intervals for the 1 hour prior to entering the scanner for the hypoxic condition.

Exposing humans to an acute hypoxic environment can be accompanied by the development of acute mountain sickness (AMS) symptoms. To track the development of this condition participants were administered the Lake Louise Questionnaire (LLQ) (Roach et al., 2018) at thirty-minute intervals throughout the experimental protocol. Clinical AMS was

defined as scoring ≥ 3 on the LLQ with the presence of headache and at least one other symptom. The presence of clinical AMS during the protocol was an exclusion criterion.

4.2.5 Anatomical MRI

All MRI sequences were conducted on a 3T Philips Ingenia Elition X (model R.5.6.1) MRI scanner (Philips Healthcare) using a 32-channel head coil. Anatomical image scans were acquired at the beginning of each scan protocol, immediately after a brief survey scan in both the normoxia and hypoxia experimental sessions. High resolution T_1-weighted images were acquired as a five-echo MP-RAGE sequence (TE = 3.5, 10.5, 20.5, 30.5, 40.5 ms; TR = 45 ms, TI = 1150 ms; 3D acquisition; field-of-view = 225 mm × 225 mm × 175 mm; voxel dimensions = 1 × 1 × 1 mm^3, SENSE = 2). The five echoes were then averaged to produce a single image used for registration of the arterial spin labelling scans, locating the HERCULES MRS acquisition voxel and subsequent tissue segmentation.

4.2.6 ASL Perfusion Imaging

To measure whole brain resting perfusion, ASL images were acquired after the structural imaging and before the acquisition of the MRS data. ASL images were acquired using the standard 3D pseudo continuous arterial spin labelling package provided with the scanner. Each scan consisted of 14 slices with a 224 X 224 mm^2 field of view (FOV) and 2 X 2 X 6 mm^3 in plane resolution. All slices were aligned perpendicular to the Z-axis of the scanner. Images were acquired as 16 matched tag and one control images with a TR = 4 s, TE = 12 ms and total scan time of 4 min 42 s. In line with the consensus recommendations, the labelling duration and post labelling delay were 1800 ms long and spectral presaturation with inversion recovery (SPIR) fat suppression was used (Alsop et al., 2015).

Image analysis was performed using the FMRIB Software Library (FSL) v6.0.5.2 MP-RAGE images were brain extracted using BET (Smith, 2002) then segmented using FAST (Zhang, Brady & Smith, 2001). ASL data were analysed using BASIL (Chappell et al., 2008), As ASL signal is dependent on blood T_1, and as blood T_1 values are dependent on haematocrit and blood oxygenation, we corrected the blood T_1 estimates used in BASIL via the model of Hales et al. (2016) for each participant using their haematocrit and SpO_2 values for each imaging session. Automatic estimation of bolus duration was applied. The CBF maps produced by BASIL were registered to the T_1-weighted structural images, smoothed with a 4-mm Gaussian kernel, masked with the grey matter image from the T_1 segmentation,

and registered to the "Montreal Neurological Institute (MNI) 2 mm" T_1-weighted average image for group comparison.

4.2.7 Edited MRS

Edited MRS were acquired using Hadamard Editing Resolves Chemicals Using Linear-combination Estimation of Spectra (HERCULES). This edited MRS technique overcomes the inherent issues of spectral overlap and low-resolution measurements of low concentration neurochemicals at three tesla field strength and below. This has been overcome by using j-difference editing techniques to untangle overlapping singles, such as *Me*scher-*Ga*rwood *P*oint *R*esolved *S*pectroscopy (MEGA-PRESS) (Mescher et al., 1998). The MEGA-PRESS acquisition involves two sub experiments within it. In the first you acquire a spectrum where you have used a selective RF-pulse to refocus the scalar coupling of the neurochemical of interest (Oeltzschner et al., 2019). You then repeat this without applying the selective RF-pulse, allowing that previously refocused coupling to freely evolve (Oeltzschner et al., 2019). The subtraction of the edit on spectrum from the edit off, nulls the signal from all neurochemicals except for that which you have applied the editing pulse too. However, the MEGA-PRESS technique is usually limited to resolving a single low concentration neurochemical over the extended acquisition period (around 10 minutes, as you doubled your traditional PRESS experiment, acquiring the edit on and off spectra). Hadamard encoded techniques, such as HERCULES, overcome this inefficiency to simultaneously edit multiple overlapping signals within a single experiment through a combination of dual editing schemes, provided the edit target is not overlapping (Chan et al., 2016). The combination can then be run across four sub experiments, not just two as in MEGA-PRESS.

This sequence allows the simultaneous editing of the low concentration Gamma-aminobutyric acid (GABA), glutathione (GSH), Lactate (Lac), Ascorbate (Asc), Aspartate (Asp) N-acetylaspartate (NAA), N-acetylaspartylglutamate (NAAG) and 2-hydroxyglutarate (2-HG), although 2-HG, an oncometabolite, is only reliably detected in tumor tissue (Oelzschner, 2019). In addition, the signals from total creatine (tCr), total choline (tCho), myo-inositol (Ins), glutamate (Glu), and glutamine (Gln) can be quantified.

The HERCULES editing scheme consists of four sub experiments, each with individual editing pulse sequences. The first is a dual-band editing scheme with an editing pulse at 4.58 ppm and 1.9 ppm. The second is again a dual-band editing scheme with the editing pulses at 4.18 and 1.9 ppm, there are two further single band editing sequences with a

single editing pulse at 4.18 ppm and 4.58 ppm. We used this exact pulse sequence in our study.

All data were acquired from within 3 x 3 x 3 cm^3 voxel positioned within the posterior cingulate cortex, using the following parameters, TR 2000 ms, TE 80 ms, collecting 320 averages (80 averages for each of the four sub experiments listed above). The total scanning time for this acquisition was 11 minutes.

HERCULES MRS data were processed and analyzed using the Osprey version 2.4.0 (Oeltzschner et al., 2020). This is an open-source software that allows preprocessing, linear combination modelling and subsequent metabolite concentration estimation with tissue correction. The Osprey pipeline produces two sub-spectra from the HERCULES data set, one combination spectra for GABA and one combination spectrum for glutathione. All default steps for HERCULES were followed in this versions pipeline. Raw Philips SDAT data were loaded into the software, automatic frequency and phase alignment, eddy-current correction, residual water removal and frequency referencing was then completed. The preprocessed spectra were then fit using Ospreys linear combination modeling and vendor specific simulated basis set across the frequency range of 0.2-4.2ppm. It included the following metabolites, Asc, Asp, Creatine (Cr), GABA, glycerphosphocholine (GPC), GSH, Gln, Glu, Ins, Lac, NAA, NAAG, phosphocholine (PCh), phosphocreatine (PCr), phosphoryl ethanolamine (PE), scyllo-inositol (sI) and Taurine (Tau). We also included the following macromolecule (MM) and lipid (Lip) basis functions in our estimations, $MM_{0.94}$, $MM_{1.22}$, $MM_{1.43}$, $MM_{1.70}$, $MM_{2.05}$, $Lip_{0.9}$, $Lip_{1.3}$, $Lip_{2.0}$.

The MRS acquisition voxel was co-registered to the individual participant's structural image. This allowed the determination of the individual tissue volume fractions for each co-registered voxel. These values were then used to correct metabolite concentration estimations for tissue specific effects of relaxation (Gasparovic et al., 2006), tissue water content and tissue metabolite content.

In our results we display both the change in the concentration of GABA and GABA+. Our acquisition scheme is a not a macromolecule suppressed scheme. The concentration of GABA we report has been created from the fitting of an experimental model of the macromolecules and the subtraction of their effect on the estimation of the concentration of GABA. This is an as yet unvalidated method to fit GABA, and so the results should be treated as preliminary, and may need further testing.

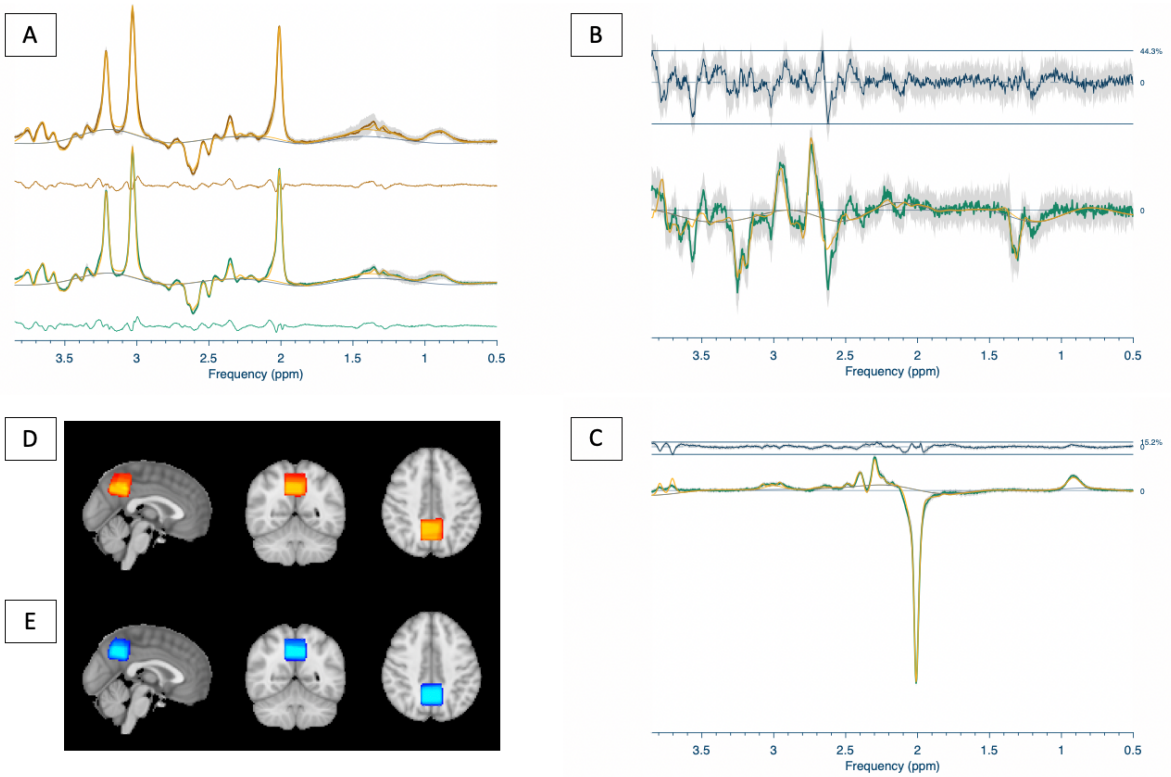

Figure 4.1. Displays the average spectra with standard deviation for normoxic and hypoxic condition, along with mean model for each and the residual (section A). Displays the average difference spectra and standard deviation (across all participants) for the calculation of glutathione, along with mean model and residual (section B). Displays the average difference spectra and standard deviation for the calculation of GABA, along with the mean model and residual (section C). The average location of the MRS acquisition voxel for the normoxic (section D) and hypoxic (section E) conditions with a 60% threshold applied, brighter colour indicates greater between participant overlap in voxel position.

4.2.8 Statistical analyses

Condition comparison of resting cerebral perfusion

A paired-samples *t*-test for whole-brain CBF changes between normoxia and hypoxia was performed in RANDOMISE (Winkler et al., 2014) (cluster mass FWE correction at $p < 0.05$). Furthermore, using the average position of the MRS voxel across participants in each condition, we extracted the mean perfusion of this region and compared between conditions.

Condition comparison of PCC neurochemicals

Metabolite concentrations quantified by Osprey were compared between normoxia and hypoxia via a paired samples T-test using Jamovi software package (R Core Team, 2019; The Jamovi Project, 2020).

4.3 Results

4.3.1 Physiology

Compared to normoxia, 1 h of poikilocapnic hypoxia increased heart rate by 11 bpm (95% CI: [17, 4]; P=0.003) and reduced peripheral arterial oxygen saturation by 13% (95%CI: [10, 15]; P<0.001).

$P_{ET}CO_2$ was measured during the acquisition of the ASL scans. In normoxia, the average (M±SD) across participants was 42±5 mmHg. After 1 hour of poikilocapnic hypoxia this slightly fell to 37±15 mmHg. This change was not significant, P=.236. See appendices K for table of physiology results.

4.3.2 Regional cerebral perfusion

Comparison of the resting state perfusion in both normoxia and hypoxia revealed that large area of the cortex exhibited an average reduction in perfusion during hypoxia. Using a cluster base analysis, significant (FWE corrected P<0.05) regions of reduced perfusion during hypoxia were found in the bilateral angular gyri and posterior cingulate gyrus (See figure 4.2)

A region of interest analysis using the mean MRS voxel location as a mask revealed that during normoxia, average CBF within the voxel was 54 ml/100g/min, this slightly fell to 53 ml/100g/min during hypoxia. This change was not significant, p=.772.

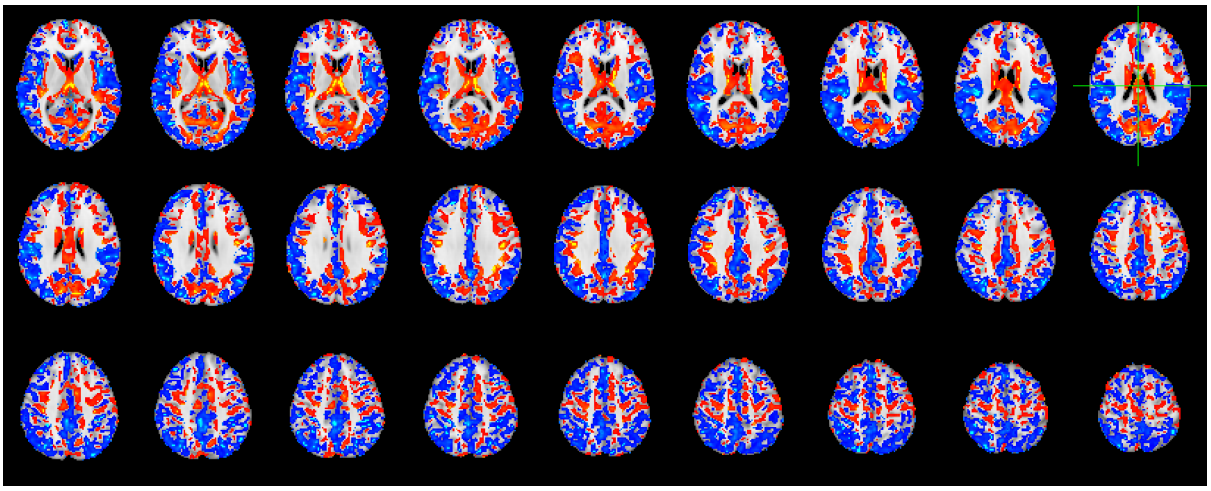

Figure 4.2. Regional resting perfusion after 1 hour of hypoxia, measured using arterial spin labelling. Red reflects average increases in perfusion across all participants, blue average

reductions. Clusters were calculated using FSL tool RANDOMISE with cluster-based thresholding and FWE correct set at $p < 0.05$

4.3.3 Magnetic Resonance Spectroscopy within the PCC

Table 1 provides a summary of the data quality metrics for the HERCULES data acquired during each condition (normoxia/hypoxia), following the MRSinMRS checklist (Lin et al., 2021).

Table 2 displays the concentration estimations for all measured metabolites in both normoxia and hypoxia. Exposure to 1 hour of hypoxia resulted in a change in the neurometabolic profile of the posterior cingulate cortex, measured whilst at rest viewing a central fixation cross. Contrary to our initial hypothesis, the concentration of GABA was found to significantly increase by 26% between normoxia and hypoxia (95% CI: [-1.11, -0.26]; $P = 0.005$; Fig 4.3.). However, when considered with the co-edited macromolecule component, the combined estimation, termed GABA+, showed non-significant 6% increase between normoxia and hypoxia (95% CI: [-1.06, -0.35]; $P = 0.300$; Appendix G.). The main excitatory neurotransmitter, glutamate showed a non-significant 8% reduction between normoxia and hypoxia (95% CI: [-0.36, 2.17]; $P = 0.144$; Appendix G), however when combined with glutamine, termed Glx, there was a 9% reduction between normoxia and hypoxia that was trending significance (95% CI: [-0.19, 2.25]; $P = 0.089$; Appendix G).

Furthermore, total choline displayed a significant 9% reduction between normoxia and hypoxia (95% CI: [0.08, 0.29]; $P = 0.002$; Appendix G) and total creatine a significant 7% reduction between normoxia and hypoxia (95% CI: [0.26, 1.32]; $P = 0.007$). Lactate was found to increase by 29% between normoxia and hypoxia (95% CI: [-0.43, -0.14]; $P = 0.001$; Appendix G).

Total NAA was found to remain stable with a non-significant 4% reduction between normoxia and hypoxia (95% CI: [-0.18, 1.77]; $P = 0.102$; Appendix G).

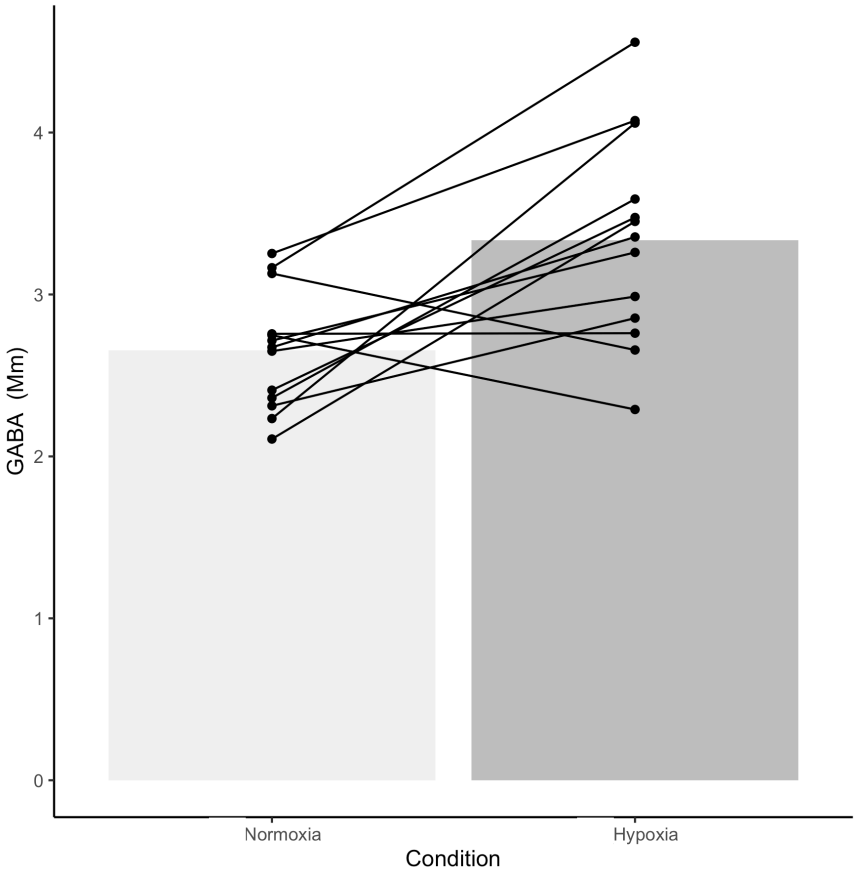

Figure 4.3. GABA concentration during normoxia (grey) and hypoxia (dark grey). Individual lines represent within participant change between conditions.

Table 4.1. Quality Measures HERCULES

	Creatine SNR	Creatine FWHM	Water FWHM	Residual Water Amplitude	Frequency Shift	Relative Residual of Sum Spectra	Relative Residual of Diff 1 Spectra	Relative Residual of Diff 2 Spectra
Normoxia	154.43	5.35	6.15	0.00	-3.03	8.06	2.33	1.66
	39.94	0.25	0.58	0.00	0.77	3.25	0.63	0.26
Hypoxia	135.83	6.13	7.16	0.00	-1.85	6.64	2.18	1.67
	33.17	0.86	1.09	0.00	1.14	2.21	0.54	0.32

Note. Smaller text below each value represents the standard deviation. Signal to noise ration of the creatine peak (Creatine SNR). Full-width-half-maximum of the creatine peak (Creatine FWHM). Full-width-half-maximum of the water peak (Water FWHM).

Table 4.2. HERCULES metabolite concentrations within the Posterior Cingulate Cortex.

	Normoxia	*SD*	*N*	*Hypoxia*	*SD*	*N*	*Δ*	*%Δ*	*P-value*	*95% CI (lower)*	*95% CI (upper)*
tNAA	19.97	1.00	13.00	19.18	1.73	13.00	-0.80	-3.98	0.102	-0.18	1.77
tCr	12.08	0.66	13.00	11.29	0.91	13.00	-0.79	-6.55	0.007*	0.26	1.32
tCho	2.07	0.12	13.00	1.88	0.18	13.00	-0.18	-8.95	0.002*	0.08	0.29
Glx	11.94	1.32	13.00	10.90	2.14	13.00	-1.03	-8.67	0.089	-0.19	2.25
mI	6.94	0.77	13.00	6.26	1.01	13.00	-0.67	-9.71	0.013*	0.17	1.18
GABA+	5.54	0.59	13.00	5.89	1.01	13.00	0.35	-6.35	0.300	-1.06	0.35
Glu	12.02	1.31	13.00	11.12	2.21	13.00	-0.90	-7.53	0.144	-0.36	2.17
Lac	0.97	0.20	13.00	1.26	0.25	13.00	0.29	29.46	0.001**	-0.43	-0.14
GABA	2.66	0.37	13.00	3.34	0.64	13.00	0.68	25.65	0.005*	-1.11	-0.26
GSH	3.12	0.66	13.00	3.10	0.44	13.00	0.02	0.76	0.906	-0.40	0.45

Note. Estimated metabolite concentrations are shown in millimolar (mM) for each condition. *SD* is the standard deviation of the mean of each metabolite in each condition. *N* is the sample size. Δ is the change in metabolite concentration from normoxia to hypoxia and Δ% is this same change expressed as a percentage. * Denotes significance at $P < .05$, ** $P < .001$. CI is the 95% confidence interval. Appendix F is a table containing the condition comparison for all fitted metabolites in this analysis.

4.4 Discussion

This investigation has utilised magnetic resonance spectroscopy to measure the neurometabolic profile of the Posterior Cingulate Cortex (PCC) after 1 hour of normobaric poikilocapnic hypoxia. We have also used pseudo-continuous arterial spin labelling to measure the resting cerebral tissue perfusion of a substantial portion of the cerebral cortex. This study has replicated previous investigations in showing a reduction in perfusion within the PCC. However, we have additionally shown an increase in neural inhibition within this region, indicated by the increase in the concentration of GABA.

4.4.1 Regional Cerebral Perfusion

As in previous studies (Rosetti et al., 2020; Lawley et al., 2017), the present findings demonstrate that after 1 hour exposure to hypoxia, the accompanying change in regional cerebral blood flow is not homogenous. Notably, the posterior portion of the cingulate gyrus and the bilateral insulas display significant reduction in perfusion during hypoxia compared to normoxia. In comparison to previous studies (Lawley et al., 2017; Rossetti et al., 2020) and chapter 2 within this thesis, the present used a shortened exposure time, with participants only experiencing the hypoxic condition for 1 hour, at the time arterial spin labelling images were acquired. Although the hypoxic stimulus severity was matched at 12 % O_2, the difference in exposure time could mean that participants are experiencing variation in their hypoxic ventilatory response and a different staging of adaption.

4.4.2 GABA

Our study has revealed after 1 hour of hypoxia, there is a significant increase in the concentration of GABA within the PCC. To the best of our knowledge, no other studies have measured human cerebral GABA concentrations using an edited MR-sequence during hypoxia. By utilising the technique in this study, we have aimed to provide a comprehensive neurometabolic profile of the PCC during hypoxia.

GABA is the primary inhibitory neurotransmitter in the human brain, through inhibiting excitation of the post synaptic membrane of neurons (Ben-Ari et al., 2012). The regional concentrations of GABA have been shown to be negatively correlated with the BOLD response amplitude (Donahue et al., 2010; Muthukumaraswamy et al., 2012) with greater concentrations conferring a greater state of tonic inhibition (Donohue et al., 2010). This relationship has been observed within the PCC, with higher resting GABA concentrations associated with greater deactivation, as measured by the BOLD response to

task engagement (Hu et al., 2013). However, others have failed to replicate this finding in the PCC (Costigan et al., 2018) and other brain regions (Harris et al., 2015). It must be remembered that when we measure the concentration of GABA, we are not solely measuring that involved in changing inhibitory neurotransmission (Stagg, Bachtiar & Johansen-Berg, 2011), to do so would involve greatly enhanced resolution capabilities. With our MRS measurement we are measuring GABA across numerous pools held within a volume of tissue, of which, the intracellular pool spread throughout the cytoplasm, rather than that held in presynaptic vesicles, is thought to be the largest and reflective of GABAs role in metabolism (Rae, 2014; Stagg et al., 2011). Therefore, changes in its concentration are reflective of changes in the levels of tonic inhibition rather than inhibitory activity per se (Rae, 2014).

The observed increase in GABA within the PCC during hypoxia is indicative of a change in inhibitory tone. We cannot exclusively state that the increase in GABA is synonymous with an increase in inhibitory neural activity as we are not exclusively resolving the GABA neurotransmitter pool (Rae, 2014). However, given GABA's modulatory effect on excitatory neurotransmission, we believe this increase reflects a shift towards a greater state of regional tonic inhibition. This is further supported by the observed trending reduction in glutamate concentration within the PCC we simultaneously measured. We would expect an alteration in the balance of excitation and inhibition to influence local heamodynamics, which would be reflective in the BOLD signal (Logothetis et al., 2001; Tagamets & Horwitz, 2001) and may provide insight to the metabolic environment of the PCC during hypoxia that underlies the reversal of the BOLD response in the Rossetti et al., 2021 investigation. However, it does not completely explain the origins of this phenomena.

There are other explanations as to why we are seeing GABA levels rise while glutamate tends to decrease. We have shown that the PCC has a reduced regional blood flow during hypoxia. Given the reduced arterial saturation of oxygen during this condition, we can assume that the delivery of oxygen to the tissues is also reduced in those areas of reduced blood flow. This anoxic environment would hamper oxidative metabolism and result in an increase in non-oxidative metabolism (glycolysis). The production of glutamate requires oxidative metabolic processes, that would be reduced within the PCC during hypoxia as a result of reduced oxygen delivery. However, the activity of the enzyme glutamic acid decarboxylase (GAD) which converts glutamate to GABA is not affected by hypoxic conditions and can withstand acidic pH conditions (Pamenter & Powell, 2016). The activity of GAD has been shown to be up regulated in the hypoxic brain (Tabata et al., 2001).

Furthermore, the degradation of GABA is also coupled to oxygen availability, hypoxic conditions and the subsequent state of acidosis would impair production of alpha-ketoglutarate required for GABA degradation (Pamenter & Powell, 2016). The net result of this could be a reduction in the concentration of glutamate as a result of sustained GAD activity, which would result in a increase in GABA concentration through this pathway which is further sustained by a reduction in its degradation as a result of the prevailing hypoxic conditions. Any proposed impact on BOLD signal, neurovascular coupling or cerebrovascular reactivity in the PCC may therefore be a by-product of these molecular mechanisms.

Finally, GABA has been shown to serve a mechanistic role in the control of the hypoxic ventilatory response in the acute phase of exposure to hypoxia (Chung et al., 2016). Antagonism of GABA receptor sites in animal models resulted in a premature ventilatory depression after acute exposure to hypoxia and lower ventilation levels (Devereaux & Pamenter, 2023). Hypoxic ventilatory depression occurs when the hypoxic exposure maintained for at least 5 minutes and is still observed up to 8 weeks if exposure is sustained (Pamenter & Powell, 2016). Therefore, GABA activity appears to have paradoxical excitatory role on the control of breathing during hypoxia (Devereaux & Pamenter, 2023). In our study, participants were exposed to at least one hour of a sustained hypoxic stimulus up until the point PCC GABA concentrations were measured. The PCC does not appear to serve a direct role in the control of breathing, however, changes in GABA concentrations during acute hypoxia may be a global effect, which could support its role in the control of the respiratory response to hypoxia, and could account for the change we see in GABA. Unfortunately, as we only investigated the one region, we cannot rule out such a global effect. Investigating the effect of hypoxia on cerebral GABA concentrations across numerous brain regions could be an avenue for future research.

4.4.3 Glutathione

The MRS sequence used in this study is optimised for the detection of low concentration metabolites, this has allowed the reliable quantification of glutathione. We found that after 1hour of hypoxia, glutathione concentration within the PCC remains unchanged. The concentrations of glutathione reported in this study are higher than the 1-2 Mm consensus but still within the range of those reported in the field (Rae & Williams, 2017). We had no hypothesis that hypoxia would alter the concentration of resting

Glutathione levels in the PCC. It is important to note that given the naturally low concentration of this metabolite in vivo, and that this investigation was conducted at only 3 tesla, our experiment would unlikely be sensitive enough to detect smaller changes on the scale of 10% (Rae & Williams, 2017).

4.4.4 Glutamate

The present study demonstrated no significant change in resting glutamate concentration between normoxia and hypoxia, replicating the resting state findings in chapter 2. This finding would prompt the conclusion that energetic demands within the PCC from excitatory neural activity are likely unchanged during hypoxia. However, at 3 tesla the separate and reliable quantification of glutamate and glutamine is difficult, without a short echo time (Wijtenburg & Knight-Scott, 2011) or asymmetric PRESS sequence (Snyder & Wilman, 2010) as such we have also chosen to analyse the combined estimation, termed Glx, which appears to show a trending reduction in concentration during hypoxia. The synthesis of glutamate during neural activity is tightly coupled to enhanced oxidative metabolism (Mangia et al., 2006, 2012; Schaller et al., 2014). This observation allows us to speculate that the trending reduction in Glx (glutamate + glutamine) in this study could reflect reduced regional metabolism or an alteration in the balance of oxidative to non-oxidative metabolism to meet regional demands. Given our observation is not a statistically significant reduction, this interpretation is only speculation requiring further exploration.

4.4.5 Lactate

We have shown cerebral lactate concentration to increase. The experiment conducted in chapter 2 of this thesis failed to reliably detect lactate. However, in the present study, the edited MRS acquisition has allowed its reliable detection. Our finding is in line with several previous studies reporting increases in cerebral lactate over varying severities of the hypoxic stimulus and durations (Edden et al., 2010; Jensen et al., 2018; Vestergaard et al., 2016; Vestergaard & Larsson, 2019). Furthermore, it has been shown that the increases in cerebral lactate measured by MRS do reflect increases in lactate generated within cerebral tissues, rather than being explained by a systemic increase in lactate during exposure to environmental hypoxia (Vestergaard et al., 2016; Harris et al., 2013).

The origins of the hypoxia-induced increase in cerebral lactate is somewhat unknown. Increased lactate has been hypothesised to reflect an up regulation of anaerobic mechanisms

to meet enhanced energy demands during hypoxia when $CMRO_2$ has been observed to increase (Vestergaard et al., 2016). However, numerous other investigations have shown $CMRO_2$ to remain stable during hypoxia, suggesting enhancements in global cerebral blood flow, maintain cerebral oxygen delivery to meet demand (Ainslie et al., 2014). Despite this stability, lactate concentration across the brain still increases (Vestergaard et al., 2022; Vestergaard & Larsson, 2017; Ainslie et al., 2014). This points towards the increase in lactate resulting from an upregulation of glycolysis in response to hypoxia as a defence mechanism (Vestergaard et al., 2022). However, without a direct measure of $CMRO_2$ in this study, we cannot rule out the role of enhanced anaerobic glycolysis to meet rising energetic demands during hypoxia.

4.4.6 Creatine

In our study we have observed a significant reduction in the measured concentration of total creatine. This finding supports previous observations by Vestergaard and Larssson (2019) and Vestergaard et al. (2016), albeit our hypoxic stimulus is less severe but for a more prolonged exposure. Nevertheless, akin to their conclusions we believe this reduction is indicative of a hypoxia-induced change in metabolism within that region. Creatine serves as an energetic buffer and plays a critical role in ATP metabolism through the Creatine-Kinase pathway (Yar, Akbar & Iqbal, 2015). In the event of a deprivation of oxygen or glucose, in the short term, metabolism of phosphocreatine in the CK-pathway allows the continued synthesis of ATP despite an environment of reduced oxygen (Balestrino et al., 2002). Furthermore, *in vitro* creatine supplementation in the rat brain, resulted in enhanced intercellular phosphocreatine concentrations and preserved synaptic transmission after 10 minutes of oxygen deprivation (Kass & Lipton, 1982). Creatine supplementation in humans resulted in a measured increase in cerebral concentrations, which preserved neurocognitive function during exposure to hypoxia, with authors concluding this to be the result of enhanced anaerobic energy provisions (Turner et al., 2015). We conclude that the hypoxia-induced reduction in creatine reflects its role of cerebral energy buffer via supporting anaerobic metabolism during hypoxia.

4.4.7 Choline

Choline is considered a marker of cell membrane density and turnover (increases in membrane synthesis or loss) (Soares & Law, 2009; Rae, 2014). Choline and phosphocholine are the precursor molecules that form cell membranes and in cholinergic neurons it is used in

the synthesis of the neurotransmitter acetylcholine (Ulus et al., 1989). Although changes in the choline resonance are primarily thought to reflect non-steady state changes in membrane turnover

However, response to an acute 20-minute period of breathing 13% oxygen, arteriovenous difference of choline concentration across the rat brain demonstrated a significant arterial increase, compared to a measured net loss during normoxia (Scremin & Jenden, 1993). Furthermore, rats that received choline dietary supplementation over a 6-month hypoxic exposure (7% oxygen) developed less pathological symptoms and had enhanced survival rates, compared to controls (Hamdorf, Cervós-Navarro & Müller, 1992). Thus, prompting the conclusion that boosting choline delivery to the brain may be neuroprotective against cerebral hypoxia.

In the present study we have shown that the total choline concentration in the cerebral tissues decreases after 1 hour of hypoxic exposure and would traditionally be interpreted as reflecting a change in membrane turnover and integrity (Rae, 2014). However, after an 8-hour 10% hypoxic exposure, serum choline was found to increase, whereas phosphocholine was reduced (Jin et al., 2010). In our study, conducted at 3 T, choline and phosphocholine cannot be reliably separated however, our measurements do indicate phosphocholine is driving the reduction whilst there is a non-significant increase in choline concentration (See Appendix F). Further investigation would be required to understand the temporal dynamics of choline metabolism during hypoxia however, we could tentatively conclude that the preservation of choline concentration could reflect a compensatory response to hypoxia that if prolonged would offer neuroprotection.

4.4.8 Myo-inositol

Myo-inositol is a component of membrane phospholipids, it is found in higher concentrations within the glial cells (Soares & Law, 2009). As such it is considered a glial marker (Soares & Law, 2009) as well as a mediator of osmoregulation (Chhetri, 2019; Soares & Law, 2009) It also serves as a post receptor and secondary cell signalling molecule (Rae, 2014). Very few investigations have looked at this neurochemical during acute periods of moderate hypoxia, akin to the physiological conditions we exposed our participants to in this investigation. The concentration of myo-inositol has been shown to reduce within the rat brain after a 48-hour 6300 meter simulated high altitude hypoxic exposure (Koundal et al., 2013). They conclude that its indicative of altered glial metabolism and enhanced cell osmolality, likely due to cerebral oedema, which they implicate due to the fact there was a

temporal elongation of T2 values within their ROIs (Koundal et al., 2013). In our study the severity of the hypoxic stimulus, and duration of exposure to it were lesser, therefore, we would not expect the development of cerebral oedema in such circumstances. However, Lawley et al. (2013) have shown that after an acute two-hour exposure to moderate hypoxia, akin to the stimulus in this study, intracellular water mobility within the white matter is reduced. They conclude a compartmental shift in water distribution, resulting in intracellular swelling, in the absence of any cerebral oedema (Lawley et al., 2013). Therefore, we can tentatively conclude that the reduction in PCC myo-inositol may be indicative of enhanced osmoregulation as a result of acute hypoxia induced intracellular swelling.

4.4.9 Conclusion

The findings of this investigation contribute to the growing body of research that has shown acute exposure to poikilocapnic hypoxia results in alteration in neurometabolism. This investigation has focused on the PCC region and has shown the concentration of GABA to be increased after a 1hour exposure to hypoxia. Our interpretation of this is that this increase reflects an up regulation of inhibitory tone within the PCC during hypoxia. The result would be a reduction in regional neuroexcitation and provides insight to the origins of the loss of activity induced increases in glutamate within this same region shown in chapter 2 of this thesis. The change in concentration of lactate, choline and creatine are indicative of metabolic stress and likely reflect regional metabolic demands being met by less efficient non-oxidative means. The present study using edited MRS techniques combined with arterial spin labelling has provided a comprehensive investigation of the neurometabolic and vascular effects of hypoxia within the PCC.

4.5 Author contribution statement.

Matthew Rogan (MR), Prof Paul Mullins (PM), Prof Sam Oliver (SO), Prof Jamie Macdonald (JM).

Project administration (MR, PM), visualisation (MR), conceptualisation (MR, PM, SO, JM), formal analysis (MR), writing of chapter (MR), review of chapter (PM, SO, JM), supervision (PM, SO, JM)

4.6 Acknowledgements

I would like to thank Joseph Smith for assistance with data acquisition, Andrew Fisher for providing MR-technician assistance and Kevin Williams for help with setup and standard protocols for hypoxia.

Chapter 5
General Discussion

5.1 Introduction

This thesis aimed to further explore what happens to the human brain upon exposure to acute and tolerable hypoxia, akin to that encountered at high altitude. Specifically, if, how and why exposure to hypoxia will alter regional cerebral blood flow and whether or not this mirrors a change in regional metabolism; which we would expect given the assumption of neurovascular-metabolic coupling.

5.2 Summary of thesis objectives

The first objective in this thesis was to replicate the findings of two previous studies (Lawley et al., 2017; Rossetti et al., 2020) that demonstrate exposure to acute poikilocapnic hypoxia does not result in uniform changes in regional cerebral blood flow across the brain. Specifically, whether posterior regions of the brain known to constitute major nodes of the default mode network (Hagmann et al., 2008), namely the posterior cingulate cortex, display reduced perfusion in response to hypoxia.

The second objective of this thesis was to utilise functional magnetic resonance spectroscopy as a non-haemodynamic dependant measure of task based neural activity within the PCC to reveal if hypoxia reverses neurovascular coupling within this region.

The third objective was to separate the effect of hypoxaemia during poikilocapnic hypoxia from the concomitant state of hypocapnia to answer whether the heterogenous changes in regional cerebral blood flow are reflective of regional sensitivities to either vascular active state.

The fourth and final objective was to use edited magnetic resonance spectroscopy to allow the acquisition of a full metabolic profile within the PCC to determine whether or not hypoxia results in a change in regional inhibitory tone.

5.3 Chapter summaries

5.3.1 Summary of key findings, chapter 2

Within chapter 2 of this thesis, we utilised arterial spin labelling to measure regional perfusion and functional magnetic resonance spectroscopy to measure changes in neurochemistry within the PCC during a memory recall task. Both measurements were taken during exposure to normoxia and hypoxia, allowing comparison between conditions.

As in previous studies (Lawley et al., 2017; Rossetti et al., 2020) we replicated the finding that after exposure to acute hypoxia, the posterior cingulate cortex displays reduced

perfusion, however, the reductions in perfusion appear to be more extensive than previously thought.

Functional MRS was able to measure an increase in glutamate concentration within the PCC during memory recall in the normoxic condition. This finding adds to the body of research already demonstrating the utility of functional MRS to measure dynamic changes in glutamate within the functioning brain (Mullins, 2018). Furthermore, it suggests the involvement of glutamatergic neurotransmission supporting the neural networks that facilitate memory recall in the human brain.

During hypoxia, there was no change in glutamate concentration during memory recall. Hypoxia negated the glutamate response but interestingly, the concentration of glucose was still found to be reduce during memory recall. Increases in glutamate concentration during neural activity are facilitated by enhanced oxidative metabolism (Mangia et al., 2006; Mangia et al., 2012; Schaller et al., 2014). We conclude that hypoxia causes a shift to non-oxidative metabolism within the PCC to sustain enhanced energy demands, disrupting the metabolism of glutamate during memory recall. This change in metabolism may also result in a regional neurovascular uncoupling, disrupting the normally attuned cerebral blood flow delivery to meet local metabolic demand.

5.3.2 Summary of key findings, chapter 3

Within chapter 3 of this thesis, we utilised arterial spin labelling to measure regional cerebral perfusion and amide proton transfer imaging, a sequence sensitive to changes in cerebral pH (Anemone et al., 2019; Zheng & Wang, 2017). Both the measurements of regional perfusion and pH were acquired during normoxia, hypoxia and a voluntary hyperventilation challenge.

Through paired comparison of each condition, we were able to show that voluntary hyperventilation resulted in a significant increase in the APT signal across the brain with concomitant global reduction in regional CBF. However, when we compared the change in the APT signal between normoxia and hypoxia and the change in CBF within the same condition, we did not find any significant overlap in the regions displaying an increase in the APT signal and reduced CBF. From this finding, we conclude that the reduction in regional CBF seen during hypoxia is not the result of a regional sensitivity to alkalosis caused by hyperventilation-induced hypocapnia during exposure to moderate hypoxia. Thus, the consistent findings in the literature (Lawley et al., 2017; Rossetti et al., 2020) and in chapter 2, 3 and 4 of this thesis, of reduced regional CBF to the PCC are not simply a reflection of a

regional sensitivity to respiratory alkalosis that develops during exposure to poikilocapnic hypoxia. There is some other mechanism that is controlling regional CBF to the PCC during hypoxia.

Interestingly, it has been shown that exposure to poikilocapnic hypoxia and the resulting hyperventilation induced hypocapnia is mechanistic in the occurrence of hypoxia induced decrements in cognitive performance. Comparison of cognitive performance during isocapnic hypoxia, hypocapnia and poikilocapnic hypoxia, found decrements in performance in all groups except for the isocapnic hypoxia, which had clamped arterial CO_2 levels, preventing the development of hyperventilation induced hypocapnia (Friend et al., 2019). Interestingly, in chapter 2, participants were experiencing a mild state of hypocapnia whilst completing the episodic memory task in hypoxia where we found performance to be reduced compared to that seen in the normoxic condition. However, in this thesis, the conclusion that this decrement in performance is the result of the prevailing state of mild hypocapnia is not explicitly made. In chapter 3 of thesis, we have shown that the posterior cingulate, a region that is explicitly involved in episodic memory recall, does not appear to be affected by the mild state of hypocapnia during poikilocapnic hypoxia as we did not detect a change in tissue pH within that region, using APT imaging. Further investigation of this result is warranted to understand the precise degree of sensitivity of APT in detecting mild pH changes with the resulting tissue alkalosis accompanying hyperventilation induced hypocapnia. This would allow us to be certain that our measurement does not lack sensitivity to any mild regional changes that we would expect during hyperventilation during poikilocapnic hypoxia. Based on our results, we would suggest that the decrement in episodic memory recall during hypoxia is not the result of hypocapnia and resulting regional tissue alkalosis and/or reduction in blood flow as result of vasoconstriction. We therefore favour the hypothesis that the hypoxia induced cognitive deficits are the result of the degree of regional hypoxaemia (Williams et al, 2019), which has been suggested as mechanistic in reduced cognitive performance, instead of hypocapnia, during exposure to poikilocapnic hypoxia.

5.3.3 Summary of key findings, chapter 4

Within chapter 4 of this thesis, we used edited magnetic resonance spectroscopy to measure the low concentration metabolites within the PCC. Numerous studies, including chapters 2, 3 and 4 in this thesis, have demonstrated regional reduction in cerebral blood flow during hypoxia. The reductions in perfusion have consistently been observed in the posterior cingulate. Previously, we measured neurochemical concentrations within the PCC, during

hypoxia whilst this region had reduced blood flow. These measurements were taken at rest and there was no significant alteration in these chemicals to suggest a change in metabolism or excitatory activity (see chapter 2). However, we were unable to acquire a full metabolic profile as the sequence used was not optimised for the detection of lower concentration metabolites, including GABA, GSH and lactate.

In chapter 4 we were able to use edited MRS (to measure a fuller metabolic profile of the PCC after exposure to acute hypoxia. As previously demonstrated (Edden et al., 2010; Jensen et al., 2018; Vestergaard et al., 2016; Vestergaard & Larsson, 2019), lactate concentration increased during hypoxia, suggesting an up-regulation of non-oxidative metabolism to meet metabolic demands during this condition. Surprisingly, GABA was found to increase in concentration during hypoxia within the PCC. Given the role of GABA as the primary inhibitory neurotransmitter within the central nervous system (Ben- Ariet al., 2012; Donohue et all., 2010; Rae, 2014) we can conclude that during hypoxia, there appears to be an increase in neuronal inhibitory tone within the PCC. This could provide an explanation for the reduction in CBF to that region as there is a suppression of excitatory neural activity. This could be indicative of an attempt to reduce metabolic demand at a region-specific level during hypoxia, in line with theories of metabolic suppression that are observed in animal models (Hochachka et al., 1996; Hochachka et al., 1999). However, the enhanced GABA concentration could also be reflective of the fact that the conversion of glutamate to GABA is maintained despite prevailing hypoxic conditions (Pamenter & Powell, 2016; Tabata et al., 2001) and degradation of GABA is reduced as it is dependent on oxidative metabolism (Pamenter & Powell, 2016). Given the prevailing hypoxaemia and the reduced blood flow to the PCC, oxidative metabolism would be down-regulated and thus any processes dependant on it, this could lead to enhancements in regional GABA concentration.

In relation to our observation in chapter two, where increases in PCC glutamate concentration associated with episodic memory recall are negated by hypoxia. We must note that our measurement of GABA concentration within the PCC was taken during the resting state, it is therefore a static measure, not capturing any functional neurochemical dynamics associated with task. This means the GABA finding is not directly translatable as they are capturing different states within the PCC. Nevertheless, assumption and speculation about the GABA finding in relation to that chapter does contribute to our understanding of the findings. In the first instance, enhancements in the concentration of GABA in the PCC, reflective of enhanced regional inhibitory tone would act as a moderator of excitatory neural activity. This could be disrupting the neural networks or enhanced neural activity that underlies episodic

memory retrieval in that region and explain the decrements in performance seen during hypoxia. However, we favour the conclusion that the reduction in glutamate concentration in chapter two is reflective of a shift to non-oxidative metabolism, rather than explicitly the result of enhanced regional inhibitory tone limiting excitatory neural activity. Further investigation is warranted to establish the precise role of GABA during functional neurochemical dynamics within the PCC during hypoxia.

5.4 Generalisability of findings

The hypoxic environment encountered at altitude involves an interaction between apposing vasoactive chemo-stimuli. As the partial pressure of arterial oxygen falls, stimulation of peripheral chemoreception drives an increase in ventilation (Steinback & Poulin, 2007). In turn, the enhanced alveolar ventilation drives a reduction in arterial CO_2 (Steinback & Poulin, 2007). If this state persists, CO_2 production by tissue metabolism is outstripped by its expulsion, resulting in respiratory alkalosis (Johnson & Morais, 2006). This aspect of hypoxia can be attenuated with CO_2 supplementation to the inhaled gas mixture to maintain constant arterial concentration of CO_2, despite enhanced alveolar ventilation. This process of clamping CO_2 arterial concentrations is described as an isocapnic hypoxic stimulus, while allowing CO_2 to vary naturally during hypoxia is termed poikilocapnic hypoxia.

Poikilocapnic hypoxia therefore allows for the simultaneous existence of two opposing chemo-stimuli, hypoxaemia promoting vasodilation and compensatory enhancements in cerebral blood flow, and hypocapnia which drives an apposing vasoconstriction (Ainslie & Poulin, 2004; Shapiro et al., 1970). Comparing cerebral blood flow measurements between poikilocapnic and isocapnic hypoxia demonstrates that hypocapnia blunts the cerebral blood flow response to hypoxaemia with a reduced magnitude and slower rate of change acutely (Ainslie & Poulin, 2004; Shapiro et al., 1970; Steinbeck & Poulin, 2016; Steinbeck & Poulin, 2008). Furthermore, it results in a regionally heterogenous CBF response, with isocapnic hypoxia resulting in concomitant CBF enhancements in the vertebral and carotid arteries but this enhancement is only observed in the vertebral arteries in poikilocapnic hypoxia (Ogoh et al., 2013). It has been reported that $CMRO_2$ is acutely increased upon exposure to hypoxia (Xu et al., 2012; Vestergaard et al., 2015) with this being mediated by hypocapnia (Ainslie, Hoiland & Bailey, 2016; Vestergaard et al., 2015; Xu et al., 2012;). It is therefore imperative in hypoxia research to distinguish between poikilocapnic and isocapnic hypoxic stimuli as both result in varying neurovascular and metabolic

responses. Furthermore, the superimposed states of hypoxaemia and hypocapnia during poikilocapnic hypoxia must be disentangled and the contributions of each to observed vascular or metabolic phenomena during poikilocapnic hypoxia.

In the acute phase, hypoxaemia results in enhancements to ventilation, cardiac output (driven by enhanced heart rate), blood pressure (Hanada, Sander & Gonzalez-Alonso, 2003), and cerebral blood flow (Kety & Schmidt, 1948; Poulin & Robbins, 1998). Concomitantly, arterial CO_2 concentrations fall with the hyperventilation and the prevailing state of hypocapnia results in a mild tissue alkalosis.

As time spent within the hypoxic environment extends beyond hours into days and weeks, alkalosis is buffered by a renally mediated prevention of bicarbonate reabsorption and secretion of hydrogen ions (Fincham et al., 2023) cerebral blood flow gradually falls to baseline levels and as period runs from weeks to years, long-term acclimatisation involves an increase in red blood cell number and haemoglobin concentration, restoring normal blood oxygen content despite the prevailing low arterial oxygen saturations (Richalet et al., 1994). Animal models of acclimatisation have also demonstrated increased capillary density (Boero et al., 1999). Duration of hypoxic exposure is therefore a critical defining feature of the neurovascular and metabolic adaptations to a hypoxic stimulus in the human brain.

The driving force behind such adaptions is an intricate molecular and cellular sensing system that detects the environmental change associated with poikilocapnic hypoxia, monitors it and initiates a cascade of intra and extra cellular adaptive processes (Sharp & Bernaudin, 2004; Terraneo & Samaja, 2017). As the duration of the hypoxic stimulus persists beyond a matter of minutes hypoxia-inducible transcription factors (HIFs) begin to mediate the expression of genes that control neuroprotective responses that allow adaption to low oxygen environment. HIFs are expressed in neurons, astrocytes and endothelial cells (Chavez et al., 2000). One such factor is HIF-1α, known to regulate genes in vascular endothelial cells (Semenza et al., 1991), regulate angiogenesis, anaerobic metabolism and mitochondrial biogenesis (Terraneo & Samaja, 2017). Its most active in acute exposures to hypoxia and is responsive to hypoxic stimulus intensity. Whereas HIF-2α, known to be expressed in capillary endothelial cells (Flamme et al., 1997), becomes increasingly active in mild hypoxic exposures that are prolonged (Terraneo & Samaja, 2017). A mutation in the gene coding this for this HIF protein is observed in Tibetan high-altitude natives and therefore is thought key to adapting to chronic hypoxic environments (Tissot Van Patot & Gassmann, 2011). Although microcellular alterations are somewhat distant from the macro-level resolution of

MRI, we cannot underestimate the relevance of changes in gene expression associated with adaption to hypoxic environments. It is clear that the duration of hypoxia, the type of hypoxia and the intensity of the hypoxic stimulus are all associated with different gene expression trajectories. Inevitably variability here will dictate or contribute to the shape and form of the vascular and metabolic adaptions to hypoxia that we are visualising using MRI and MRS in this thesis.

When considering the generalisability of the findings in this thesis, care must be taken to ensure the time spent in hypoxia, the type of hypoxic stimulus and its intensity are considered. Interestingly, we have observed a consistent inter participant variability across all studies in this thesis. For example, while the majority of participants showed a reduction in glutamate concentration in hypoxia during the fMRS task in chapter 2, some participant showed the opposite trend, displaying an increase, akin to their normoxic response. Furthermore, the finding that posterior cingulate GABA concentrations are increased during hypoxia is not absolute for our sample. Inherent in our study design is a blindness to oxygen saturations while participants were within the scanner. Therefore, we cannot confirm the precise degree of hypoxaemia each person was experiencing as the MRS data were acquired. Having such measurements could allow insight to variability between participants in oxygen saturations and how varying degrees of hypoxaemia may account for the observed metabolic changes. Furthermore, similar investigations to ours that have exposed participants to at least 1 hour of moderate hypoxic stimulus have seen variability in cerebral glutamate concentration (Vestergaard et al., 2016) and global measures of $CMRO_2$ (Smith et al., 2013; Vestergaard et al., 2016; Wang et al., 2015). They hypothesise that this variability results from inter-participant differences in the hypoxic ventilatory response and the degree of hypocapnia experienced (Vestergaard et al., 2016). We have not measured breathing rate or time course of change in expired gases in response to hypoxic exposure therefore cannot look specifically at inter-participant variability in the hypoxic ventilatory response and how that relates to any metabolic or vascular variability we observe, but this would be an interesting idea for future research proposals.

5.5 Limitations

The human brain is highly regionally organised, specialised, and distinct. Not only will a given region be different because of the connections it boasts to other regions, but also in cell type, density, vascularisation, neurotransmission and metabolism. The Posterior Cingulate Cortex is one such region. It is highly anatomically connected compared to other

brain regions, indicative of its role as a major hub or node supporting brain function (Hagmann et al., 2008). It forms a central node of the default mode network (Raichle et al., 2001). However, there is no clear consensus on its core functions (Leech, Braga & Sharp, 2012). Strikingly, the PCC has a high baseline metabolic rate and cerebral blood flow relative to other brain regions (Raichle et al., 2001). Interestingly, relative changes in activity measured by changes in metabolism within the region are not met with corresponding changes in CBF, which are distinctively less clear and more marginal (Raichle et al., 2001). Appreciating the distinct regionality within the human brain, and particularly the phenotype of the PCC, reveals an area of caution and limitation to the investigation within this thesis. Although we utilised imaging techniques that can provide whole brain regional data, such as arterial spin labelling, we have also used techniques that have a limited regional resolution such as our MRS experiments. This limits our understanding and application of findings to the specific region studied.

Upon exposure to poikilocapnic hypoxia, the hypoxic ventilatory response, which is known to significantly vary between individuals, will result in varying degrees of hyperventilation induced hypocapnia. During acute exposures, this allows for the co-existence of hypoxaemia and hypocapnia, two opposing chemo stimuli with one triggering the relaxation of vascular smooth muscle, whilst the other stimulate contraction. In chapter 3 of this thesis, we attempted to examine whether or not, hypocapnia could account for the regional reduction in CBF during acute hypoxia. However, to do this we took the difficult task of simulating hypocapnia and comparing measures of CBF and APT between this state and during acute hypoxia. It is important to note that we could not produce the exact matching levels of hypocapnia in this study, with considerable intra person variability. There are now techniques available that enable the clamping of end-tidal gases through CO_2 supplementation. Such a procedure would allow the examination of the sole role of hypoxaemia on regional cerebral blood flow and metabolism and would be a more precise technique to examine the mechanistic relationship between these observations.

Within this thesis we have aimed to investigate whether the observation of a reversed BOLD signal to task within the PCC during hypoxia, is in fact the result in a hypoxia induced reversal in neurovascular coupling. Rossetti et al. (2020) observed a reversal of the BOLD signal within the PCC in both a task that typically elicits a positive BOLD signal and task that elicits a negative BOLD signal. We have used a novel fMRS paradigm to measure neurometabolism within the PCC during a memory recall task. This task is typically associated with a positive BOLD response within this region, but hypoxia reversed this,

resulting a negative BOLD response. We did not investigate the origins of the reversal of a negative BOLD response to a positive BOLD response within the PCC during a spatial attention task. The mechanisms that underlie the negative BOLD response are different to those that underlie the positive BOLD response. Given this, we cannot assume the observation we have made would translate. Investigating the dynamic neurochemical changes to both types of tasks would provide a more comprehensive understanding to the neurovascular and metabolic changes within the PCC during hypoxia.

In all experiments within this thesis, we have taken physiological measurements at set intervals, these include, heart rate, blood pressure, peripheral saturations and end tidal CO_2 measurements. These measurements were taken at set interval frequencies in both normoxic and hypoxic conditions until the point at which the participants entered the MR environment. After the point the participants entered the MR environment, the only measurement that could be taken was the end tidal CO_2. This was due to a lack of MR safe monitoring equipment for our investigations. We have therefore operated on an assumption that heart rate, blood pressure and oxygen saturations would remain unchanged for the period the participants were within the MR environment. While in the scanner participants wore a leak free air mask and breathed hypoxic air, each person masks were fitted to them and checked for leakage prior to entering. Although there is no significant reason to suspect a significant change in these physiological variables, we cannot negate there being variation that could account for some of the inter-participant differences we observed.

5.6 Implications and future directions

This thesis has demonstrated the use of a novel event-related functional MRS paradigm in measuring dynamic changes in neurometabolites. We have been able to successfully measure a functional change in glutamate concentration within the posterior cingulate during memory recall. These findings further build on the reliability of using fMRS to understand the functioning human brain and suggest the involvement of glutamate neurotransmission and metabolism within the PCC facilitating memory recall.

Building from this we have demonstrated that acute hypoxia nullifies the glutamate response during memory recall, possibly reflecting a reduction in glutamate neurotransmission and a shift to non-oxidative metabolism within the region. Given that most participants also demonstrated reduced memory recall performance, this implicates the impaired or altered glutamate neurotransmission and metabolism, particularly within the PCC, as a driver for impaired memory recall. This has wider applications to future work

focused on understanding the mechanism of impaired memory recall and vulnerability of the posterior cingulate in brain injury and disease.

Within chapter three of this thesis, we have used a novel amide proton transfer imaging sequence as means of measuring changes in tissue pH, that occur with respiratory alkalosis. APT imaging is a form of chemical exchange saturation transfer imaging (Anemone et al., 2019), the technique is sensitive to tissue pH (Ward & Balaban, 2000) and has traditionally been used in the imaging of tumours or ischaemic penumbra (Zhou et al., 2003) to distinguish between healthy and diseased tissues. Here we have used it to image a mild change in pH that occurs with respiratory alkalosis as a result of voluntary hyperventilation. We have shown this technique to be sensitive to such changes, as displayed in the figures within chapter 3. This demonstrates the utility and flexibility of this technique in studying the healthy brain exposed to extreme environments. However, going forward, we propose research to focus on the validity and precise sensitivity of this technique to tolerable changes in tissue pH. This could be conducted by using the APT weighted imaging in a paradigm of stepped changes in end tidal CO_2 and comparison with other more routine cerebral tissue pH measurements such as those using MRS (Zhou et al., 2003).

5.7 Concluding statement

We return to our initial thesis aim, to ascertain whether changes we see in regional cerebral blood flow are the result of metabolic, functional or physiological (vascular response to blood gas changes) effectors during environmental hypoxia.

From the investigations within this thesis, we can conclude the following. The reductions in regional cerebral blood flow, that have been observed consistently within the PCC are not simply the result of a regional sensitivity to hypocapnia, a state that is incurred during hypoxia induced hyperventilation. Furthermore, we do not propose that this same region displays a reversal in neurovascular coupling, with activity stimulating a reduction in blood flow, but instead a neurovascular uncoupling. This is likely the result of a shift in the balance of oxidative and non-oxidative metabolism, in favour of non-oxidative. This would disrupt excitatory neurotransmission and inevitably the signalling pathways that govern neurovascular coupling. One mechanism for this could be an enhancement in neuro-inhibitory tone within this region, as chapter 4 of this thesis suggests, with the observed increase in PCC GABA during hypoxia. However, from our data, we would not be able to ascertain whether the increase in GABA during hypoxia is driving the reductions in blood

flow or, if it is increased as a result of neurovascular uncoupling and forms a defensive mechanism in the face of reduced blood flow.

Reference List

Ainslie, P. N., Hoiland, R. L., & Bailey, D. M. (2016). Lessons from the laboratory; integrated regulation of cerebral blood flow during hypoxia. *Experimental physiology*, *101*(9), 1160-1166.

Ainslie, P. N., & Poulin, M. J. (2004). Ventilatory, cerebrovascular, and cardiovascular interactions in acute hypoxia: regulation by carbon dioxide. *Journal of applied physiology*, *97*(1), 149-159.

Ainslie, P. N., Shaw, A. D., Smith, K. J., Willie, C. K., Ikeda, K., Graham, J., & Macleod, D. B. (2014). Stability of cerebral metabolism and substrate availability in humans during hypoxia and hyperoxia. *Clinical Science*, *126*(9), 661–670. https://doi.org/10.1042/CS20130343

Ainslie, P. N., & Subudhi, A. W. (2014). Cerebral blood flow at high altitude. *High altitude medicine & biology*, *15*(2), 133-140.

Andrews-Hanna, J. R., Snyder, A. Z., Vincent, J. L., Lustig, C., Head, D., Raichle, M. E., & Buckner, R. L. (2007). Disruption of large-scale brain systems in advanced aging. *Neuron*, *56*(5), 924-935.

Alsop, D. C., Detre, J. A., Golay, X., Günther, M., Hendrikse, J., Hernandez-Garcia, L., ... & Zaharchuk, G. (2015). Recommended implementation of arterial spin-labeled perfusion MRI for clinical applications: a consensus of the ISMRM perfusion study group and the European consortium for ASL in dementia. *Magnetic resonance in medicine*, *73*(1), 102-116.

Anemone, A., Consolino, L., Arena, F., Capozza, M., & Longo, D. L. (2019). Imaging tumor acidosis: a survey of the available techniques for mapping in vivo tumor pH. *Cancer and Metastasis Reviews*, *38*, 25-49.

Apšvalka, D., Gadie, A., Clemence, M., & Mullins, P. G. (2015). Event-related dynamics of glutamate and BOLD effects measured using functional magnetic resonance spectroscopy (fMRS) at 3T in a repetition suppression paradigm. *NeuroImage*, *118*, 292–300. https://doi.org/10.1016/j.neuroimage.2015.06.015

Balestrino, M., Lensman, M., Parodi, M., Perasso, L., Rebaudo, R., Melani, R., ... & Cupello, A. (2002). Role of creatine and phosphocreatine in neuronal protection from anoxic and ischemic damage. *Amino Acids*, *23*(1), 221-229.

Bednařík, P., Tkáč, I., Giove, F., Dinuzzo, M., Deelchand, D. K., Emir, U. E., … Mangia, S. (2015). Neurochemical and BOLD responses during neuronal activation measured in

the human visual cortex at 7 Tesla. *Journal of Cerebral Blood Flow and Metabolism*, *35*(October 2014), 601–610. https://doi.org/10.1038/jcbfm.2014.233

Berg, M. D., & Meyer, R. J. (Eds.). (2008). Chapter 14—Gas Exchange and Acid-Base Physiology. In *Pediatric Respiratory Medicine (Second Edition)* (Second Edition, pp. 179–200). Mosby. https://doi.org/10.1016/B978-032304048-8.50018-9

Ben-Ari, Y., Khalilov, I., Kahle, K. T., & Cherubini, E. (2012). The GABA excitatory/inhibitory shift in brain maturation and neurological disorders. *The Neuroscientist*, *18*(5), 467-486.

Binks, A. P., Cunningham, V. J., Adams, L., & Banzett, R. B. (2008). Gray matter blood flow change is unevenly distributed during moderate isocapnic hypoxia in humans. *Journal of Applied Physiology*, *104*(1), 212–217. https://doi.org/10.1152/japplphysiol.00069.2007

Boero, J. A., Ascher, J., Arregui, A., Rovainen, C., & Woolsey, T. A. (1999). Increased brain capillaries in chronic hypoxia. *Journal of applied physiology*, *86*(4), 1211-1219.

Boillat, Y., Xin, L., van der Zwaag, W., & Gruetter, R. (2020). Metabolite concentration changes associated with positive and negative BOLD responses in the human visual cortex: A functional MRS study at 7 Tesla. *Journal of Cerebral Blood Flow and Metabolism*, *40*(3), 488–500. https://doi.org/10.1177/0271678X19831022

Boly, M., Phillips, C., Tshibanda, L., Vanhaudenhuyse, A., Schabus, M., Dang-Vu, T. T., ... & Laureys, S. (2008). Intrinsic brain activity in altered states of consciousness: how conscious is the default mode of brain function?. *Annals of the New York Academy of Sciences*, *1129*(1), 119-129.

Borchers, H.W. pracma: Practical Numerical Math Functions. R package version 2.3.3. https://CRAN.R-project.org/package=pracma (accessed January 2021).

Brainard, D.H. (1997). The psychophysics toolbox. Spat Vis; 10: 433–436.

Buck, A., Schirlo, C., Jasinsky, V., Weber, B., Burger, C., von Schulthess, G. K., ... & Pavlicek, V. (1998). Changes of cerebral blood flow during short-term exposure to normobaric hypoxia. *Journal of Cerebral Blood Flow & Metabolism*, *18*(8), 906-910.

Buckner, R. L., Andrews-Hanna, J. R., & Schacter, D. L. (2008). The brain's default network: anatomy, function, and relevance to disease. *Annals of the new York Academy of Sciences*, *1124*(1), 1-38.

Buckner, R. L., Sepulcre, J., Talukdar, T., Krienen, F. M., Liu, H., Hedden, T., ... & Johnson, K. A. (2009). Cortical hubs revealed by intrinsic functional connectivity: mapping,

assessment of stability, and relation to Alzheimer's disease. *Journal of neuroscience*, *29*(6), 1860-1873.

Carlson, G. P., & Bruss, M. (2008). Chapter 17—Fluid, Electrolyte, and Acid-Base Balance. In J. J. Kaneko, J. W. Harvey, & M. L. Bruss (Eds.), *Clinical Biochemistry of Domestic Animals (Sixth Edition)* (Sixth Edition, pp. 529–559). Academic Press. https://doi.org/10.1016/B978-0-12-370491-7.00017-9

Chappell, M. A., Groves, A. R., Whitcher, B., & Woolrich, M. W. (2008). Variational Bayesian inference for a nonlinear forward model. *IEEE Transactions on Signal Processing*, *57*(1), 223-236.

Chhetri, D. R. (2019). Myo-inositol and its derivatives: their emerging role in the treatment of human diseases. *Frontiers in pharmacology*, *10*, 1172.

Chan, K. L., Puts, N. A., Schär, M., Barker, P. B., & Edden, R. A. (2016). HERMES: Hadamard encoding and reconstruction of MEGA-edited spectroscopy. *Magnetic resonance in medicine*, *76*(1), 11-19.

Chavez, J. C., Agani, F., Pichiule, P., & LaManna, J. C. (2000). Expression of hypoxia-inducible factor-1α in the brain of rats during chronic hypoxia. *Journal of applied physiology*, *89*(5), 1937-1942.

Chung, D., Dzal, Y. A., Seow, A., Milsom, W. K., & Pamenter, M. E. (2016). Naked mole rats exhibit metabolic but not ventilatory plasticity following chronic sustained hypoxia. *Proceedings of the Royal Society B: Biological Sciences*, *283*(1827), 20160216.

Cohen, P. J., Alexander, S. C., Smith, T. C., Reivich, M. A. R. T. I. N., & Wollman, H. A. R. R. Y. (1967). Effects of hypoxia and normocarbia on cerebral blood flow and metabolism in conscious man. *Journal of Applied Physiology*, *23*(2), 183-189.

Costigan, A. G., Umla-Runge, K., Evans, C. J., Hodgetts, C. J., Lawrence, A. D., & Graham, K. S. (2019). Neurochemical correlates of scene processing in the precuneus/posterior cingulate cortex: A multimodal fMRI and 1H-MRS study. *Human brain mapping*, *40*(10), 2884-2898.

Devereaux, M. E., & Pamenter, M. E. (2023). Adenosine and γ-aminobutyric acid partially regulate metabolic and ventilatory responses of Damaraland mole-rats to acute hypoxia. *Journal of Experimental Biology*, *226*(19).

Donahue, M. J., Near, J., Blicher, J. U., & Jezzard, P. (2010). Baseline GABA concentration and fMRI response. *Neuroimage*, *53*(2), 392-398.

Duncombe, J., Lennen, R. J., Jansen, M. A., Marshall, I., Wardlaw, J. M., & Horsburgh, K. (2017). Ageing causes prominent neurovascular dysfunction associated with loss of astrocytic contacts and gliosis. *Neuropathology and applied neurobiology*, *43*(6), 477-491.

Edden, R. A. E., Harris, A. D., Murphy, K., Evans, C. J., Saxena, N., Hall, J. E., … Wise, R. G. (2010). Edited MRS is sensitive to changes in lactate concentration during inspiratory hypoxia. *Journal of Magnetic Resonance Imaging*, *32*(2), 320–325. https://doi.org/10.1002/jmri.22233

Fan, J. L., Burgess, K. R., Basnyat, R., Thomas, K. N., Peebles, K. C., Lucas, S. J., ... & Ainslie, P. N. (2010). Influence of high altitude on cerebrovascular and ventilatory responsiveness to CO2. *The Journal of physiology*, *588*(3), 539-549.

Fincham, G. W., Kartar, A., Uthaug, M. V., Anderson, B., Hall, L., Nagai, Y., ... & Colasanti, A. (2023). High ventilation breathwork practices: An overview of their effects, mechanisms, and considerations for clinical applications. *Neuroscience & Biobehavioral Reviews*, 105453.

Flamme, I., Fröhlich, T., von Reutern, M., Kappel, A., Damert, A., & Risau, W. (1997). HRF, a putative basic helix-loop-helix-PAS-domain transcription factor is closely related to hypoxia-inducible factor-1α and developmentally expressed in blood vessels. *Mechanisms of development*, *63*(1), 51-60.

Gasparovic, C., Song, T., Devier, D., Bockholt, H. J., Caprihan, A., Mullins, P. G., ... & Morrison, L. A. (2006). Use of tissue water as a concentration reference for proton spectroscopic imaging. *Magnetic Resonance in Medicine: An Official Journal of the International Society for Magnetic Resonance in Medicine*, *55*(6), 1219-1226.

Greicius, M. D., Supekar, K., Menon, V., & Dougherty, R. F. (2009). Resting-state functional connectivity reflects structural connectivity in the default mode network. *Cerebral cortex*, *19*(1), 72-78.

Grocott, M. P., Martin, D. S., Levett, D. Z., McMorrow, R., Windsor, J., & Montgomery, H. E. (2009). Arterial blood gases and oxygen content in climbers on Mount Everest. *New England Journal of Medicine*, *360*(2), 140-149.

Gusnard, D. A., & Raichle, M. E. (2001). Searching for a baseline: functional imaging and the resting human brain. *Nature reviews neuroscience*, *2*(10), 685-694.

Hagmann, P., Cammoun, L., Gigandet, X., Meuli, R., Honey, C. J., Wedeen, V. J., & Sporns, O. (2008). Mapping the structural core of human cerebral cortex. *PLoS biology*, *6*(7), e159.

Hales, P. W., Kirkham, F. J., & Clark, C. A. (2016). A general model to calculate the spin-lattice (T1) relaxation time of blood, accounting for haematocrit, oxygen saturation and magnetic field strength. *Journal of cerebral blood flow and metabolism : official journal of the International Society of Cerebral Blood Flow and Metabolism*, *36*(2), 370–374. https://doi.org/10.1177/0271678X15605856

Hahn, B., Ross, T. J., & Stein, E. A. (2007). Cingulate activation increases dynamically with response speed under stimulus unpredictability. *Cerebral cortex*, *17*(7), 1664-1671.

Hamdorf, G., Cervos-Navarro, J., & Müller, R. (1992). Increase of survival time in experimental hypoxia by cytidine diphosphate choline. *Arzneimittel-forschung*, *42*(4), 421-424.

Hanada, A., Sander, M., & González-Alonso, J. (2003). Human skeletal muscle sympathetic nerve activity, heart rate and limb haemodynamics with reduced blood oxygenation and exercise. *The Journal of physiology*, *551*(2), 635-647.

Harris, A. D., Puts, N. A., Anderson, B. A., Yantis, S., Pekar, J. J., Barker, P. B., & Edden, R. A. (2015). Multi-regional investigation of the relationship between functional MRI blood oxygenation level dependent (BOLD) activation and GABA concentration. *PloS one*, *10*(2), e0117531.

Harris, A. D., Roberton, V. H., Huckle, D. L., Saxena, N., Evans, C. J., Murphy, K., Hall, J. E., Bailey, D. M., Mitsis, G., Edden, R. A. E., & Wise, R. G. (2013). Temporal dynamics of lactate concentration in the human brain during acute inspiratory hypoxia. *Journal of Magnetic Resonance Imaging*, *37*(3), 739–745. https://doi.org/10.1002/jmri.23815

Hochachka, P. W., Clark, C. M., Matheson, G. O., Brown, W. D., Stone, C. K., Nickles, R. J., & Holden, J. E. (1999). Effects on regional brain metabolism of high-altitude hypoxia: a study of six US marines. *American Journal of Physiology-Regulatory, Integrative and Comparative Physiology*, *277*(1), R314–R319. https://doi.org/10.1152/ajpregu.1999.277.1.r314

Hochachka, P. W., Clark, C. M., Monge, C., Stanley, C., Brown, W. D., Stone, C. K., … Holden, J. E. (1996). Sherpa brain glucose metabolism and defense adaptations against chronic hypoxia. *Journal of Applied Physiology*, *81*(3), 1355–1361. https://doi.org/10.1152/jappl.1996.81.3.1355

Hu, Y., Chen, X., Gu, H., & Yang, Y. (2013). Resting-state glutamate and GABA concentrations predict task-induced deactivation in the default mode network. *Journal of Neuroscience*, *33*(47), 18566-18573.

Imray, C., Chan, C., Stubbings, A., Rhodes, H., Patey, S., Wilson, M. H., ... & Birmingham Medical Research Expeditionary Society. (2014). Time course variations in the mechanisms by which cerebral oxygen delivery is maintained on exposure to hypoxia/altitude. *High altitude medicine & biology*, *15*(1), 21-27.

Ip, I. B., Berrington, A., Hess, A. T., Parker, A. J., Emir, U. E., & Bridge, H. (2017). Combined fMRI-MRS acquires simultaneous glutamate and BOLD-fMRI signals in the human brain. *Neuroimage*, *155*, 113-119. https://doi.org/10.1016/j.neuroimage.2017.04.030

Ip, I. B., Emir, U. E., Parker, A. J., Campbell, J., & Bridge, H. (2019). Comparison of neurochemical and BOLD signal contrast response functions in the human visual cortex. *Journal of Neuroscience*, *39*(40), 7968-7975.

Ito, H., Ibaraki, M., Kanno, I., Fukuda, H., & Miura, S. (2005). Changes in the arterial fraction of human cerebral blood volume during hypercapnia and hypocapnia measured by positron emission tomography. *Journal of Cerebral Blood Flow & Metabolism*, *25*(7), 852-857.

Jenkinson, M., Bannister, P., Brady, M., & Smith, S. (2002). Improved optimization for the robust and accurate linear registration and motion correction of brain images. *Neuroimage*, *17*(2), 825-841.

Jenkinson, M., & Smith, S. (2001). A global optimisation method for robust affine registration of brain images. *Medical image analysis*, *5*(2), 143-156.

Jensen, M. L. F., Vestergaard, M. B., Tønnesen, P., Larsson, H. B. W., & Jennum, P. J. (2018). Cerebral blood flow, oxygen metabolism, and lactate during hypoxia in patients with obstructive sleep apnea. *Sleep*, *41*(3), zsy001.

Jin, L. I. U., Jian-Quan, W. U., Ji-Jun, Y. A. N. G., Jing-Yu, W. E. I., Wei-Na, G. A. O., & Chang-Jiang, G. U. O. (2010). Metabolomic study on vitamins B1, B2, and pp supplementation to improve serum metabolic profiles in mice under acute hypoxia based on 1h nmr analysis. *Biomedical and Environmental Sciences*, *23*(4), 312-318.

Johnson, K. A., Jones, K., Holman, B. L., Becker, J. A., Spiers, P. A., Satlin, A., & Albert, M. S. (1998). Preclinical prediction of Alzheimer's disease using SPECT. *Neurology*, *50*(6), 1563-1571.

Johnson, R. A., & Morais, H. A. D. (2006). Respiratory acid–base disorders. *Fluid, Electrolyte, and Acid–base Disorders in Small Animal Practice*.

Kass, I. S., & Lipton, P. (1982). Mechanisms involved in irreversible anoxic damage to the in vitro rat hippocampal slice. *The Journal of Physiology*, *332*(1), 459-472.

Kassambara, A. (2020). rstatix: Pipe-Friendly Framework for Basic Statistical Tests. R package version 0.6.0. Available from https://CRAN.R-project.org/package=rstatix

Kety, S. S., & Schmidt, C. F. (1948). The effects of altered arterial tensions of carbon dioxide and oxygen on cerebral blood flow and cerebral oxygen consumption of normal young men. *The Journal of clinical investigation*, *27*(4), 484-492.

Koundal, S., Gandhi, S., Kaur, T., & Khushu, S. (2014). Neurometabolic and structural alterations in rat brain due to acute hypobaric hypoxia: in vivo 1H MRS at 7 T. *NMR in Biomedicine*, *27*(3), 341-347.

Kozberg, M. G., Chen, B. R., DeLeo, S. E., Bouchard, M. B., & Hillman, E. M. (2013). Resolving the transition from negative to positive blood oxygen level-dependent responses in the developing brain. *Proceedings of the National Academy of Sciences*, *110*(11), 4380-4385.

Kozberg, M., & Hillman, E. (2016). Neurovascular coupling and energy metabolism in the developing brain. https://doi.org/10.1016/bs.pbr.2016.02.002

Kusaka, T., Kawada, K., Okubo, K., Nagano, K., Namba, M., Okada, H., ... & Itoh, S. (2004). Noninvasive optical imaging in the visual cortex in young infants. *Human brain mapping*, *22*(2), 122-132.

Lally, N., Mullins, P. G., Roberts, M. V., Price, D., Gruber, T., & Haenschel, C. (2014). Glutamatergic correlates of gamma-band oscillatory activity during cognition: A concurrent ER-MRS and EEG study. *NeuroImage*, *85*, 823–833. https://doi.org/10.1016/j.neuroimage.2013.07.049

Lawley, J. S., Oliver, S. J., Mullins, P. G., & Macdonald, J. H. (2013). Investigation of whole-brain white matter identifies altered water mobility in the pathogenesis of high-altitude headache. *Journal of Cerebral Blood Flow & Metabolism*, *33*(8), 1286-1294.

Lawley, J. S., Macdonald, J. H., Oliver, S. J., & Mullins, P. G. (2017). Unexpected reductions in regional cerebral perfusion during prolonged hypoxia. *Journal of Physiology*, *595*(3). https://doi.org/10.1113/JP272557

Leech, R., Braga, R., & Sharp, D. J. (2012). Echoes of the brain within the posterior cingulate cortex. *Journal of Neuroscience*, *32*(1), 215-222.

Leech, R., Kamourieh, S., Beckmann, C. F., & Sharp, D. J. (2011). Fractionating the default mode network: distinct contributions of the ventral and dorsal posterior cingulate cortex to cognitive control. *Journal of Neuroscience*, *31*(9), 3217-3224.

Leech, R., & Sharp, D. J. (2014). The role of the posterior cingulate cortex in cognition and disease. *Brain*, *137*(1), 12-32.

Leech, R., & Smallwood, J. (2019). The posterior cingulate cortex: Insights from structure and function. *Handbook of clinical neurology*, *166*, 73-85.

Lenth, R. (2018). Emmeans: Estimates Marginal Means, aka Least-Squares Means. [computer software]. Retrieved from: https://cran.r-project.org/package=emmeans.

Lewis, N. C., Messinger, L., Monteleone, B., & Ainslie, P. N. (2014). Effect of acute hypoxia on regional cerebral blood flow: effect of sympathetic nerve activity. *Journal of applied physiology*, *116*(9), 1189-1196.

Logothetis, N. K., Pauls, J., Augath, M., Trinath, T., & Oeltermann, A. (2001). Neurophysiological investigation of the basis of the fMRI signal. *nature*, *412*(6843), 150-157.

Logothetis, N. K. (2008). What we can do and what we cannot do with fMRI. *Nature*, *453*(7197), 869–878. https://doi.org/10.1038/nature06976

Lyros, E., Ragoschke-Schumm, A., Kostopoulos, P., Sehr, A., Backens, M., Kalampokini, S., ... & Fassbender, K. (2020). Normal brain aging and Alzheimer's disease are associated with lower cerebral pH: an in vivo histidine 1H-MR spectroscopy study. *Neurobiology of aging*, *87*, 60-69.

Margulies, D. S., Vincent, J. L., Kelly, C., Lohmann, G., Uddin, L. Q., Biswal, B. B., ... & Petrides, M. (2009). Precuneus shares intrinsic functional architecture in humans and monkeys. *Proceedings of the National Academy of Sciences*, *106*(47), 20069-20074.

Makowski, D. (2018). The Psycho Package: An Efficient and Publishing-Oriented Workflow for Psychological Science. Journal of Open Source Software, 3(22), 470. Available from https://github.com/neuropsychology/psycho.R

Mangia, S., Giove, F., & DiNuzzo, M. (2012). Metabolic pathways and activity-dependent modulation of glutamate concentration in the human brain. *Neurochemical Research*, *37*(11), 2554–2561. https://doi.org/10.1007/s11064-012-0848-4

Mangia, S., Tkáč, I., Gruetter, R., Van De Moortele, P. F., Giove, F., Maraviglia, B., & Uğurbil, K. (2006). Sensitivity of single-voxel 1H-MRS in investigating the metabolism of the activated human visual cortex at 7 T. *Magnetic Resonance Imaging*, *24*(4), 343–348. https://doi.org/10.1016/j.mri.2005.12.023

Martínez-Maestro, M., Labadie, C., & Möller, H. E. (2018). Dynamic metabolic changes in human visual cortex in regions with positive and negative blood oxygenation level-dependent response. *Journal of Cerebral Blood Flow & Metabolism*, 0271678X1879542. https://doi.org/10.1177/0271678X18795426

Merz, T. M., Treyer, V., Hefti, U., Spengler, C. M., Schwarz, U., Buck, A., & Maggiorini, M. (2006). Changes in cerebral glucose metabolism after an expedition to high altitudes. *High altitude medicine & biology*, *7*(1), 28-38.

Mescher, M., Merkle, H., Kirsch, J., Garwood, M., & Gruetter, A. R. (1998). Simultaneous in vivo spectral editing and water suppression. *NMR in Biomedicine: An International Journal Devoted to the Development and Application of Magnetic Resonance In Vivo*, *11*(6), 266-272.

Milroy, C. M. (2018). Deaths from environmental hypoxia and raised carbon dioxide. *Academic forensic pathology*, *8*(1), 2-7.

Mullins, P. G. (2018). Towards a theory of functional magnetic resonance spectroscopy (fMRS): A meta-analysis and discussion of using MRS to measure changes in neurotransmitters in real time. https://doi.org/10.1111/sjop.12411

Mullins, P. G., Chen, H., Xu, J., Caprihan, A., & Gasparovic, C. (2008). Comparative reliability of proton spectroscopy techniques designed to improve detection of J-coupled metabolites. *Magnetic Resonance in Medicine*, *60*(4), 964–969. https://doi.org/10.1002/mrm.21696

Muthukumaraswamy, S. D., Evans, C. J., Edden, R. A., Wise, R. G., & Singh, K. D. (2012). Individual variability in the shape and amplitude of the BOLD-HRF correlates with endogenous GABAergic inhibition. *Human brain mapping*, *33*(2), 455-465.

Naressi, A., Couturier, C., Devos, J. M., Janssen, M., Mangeat, C., de Beer, R., & Graveron-Demilly, D. (2001). jMRUI, MRUI for Java. *MAGMA*, *12*, 141-152.

Noble, J., Jones, J. G., & Davis, E. J. (1993). Cognitive function during moderate hypoxaemia. *Anaesthesia and Intensive Care*, *21*(2), 180-184.

Nöth, U., Kotajima, F., Deichmann, R., Turner, R., & Corfield, D. R. (2008). Mapping of the cerebral vascular response to hypoxia and hypercapnia using quantitative perfusion MRI at 3 T. *NMR in Biomedicine*, *21*(5), 464–472. https://doi.org/10.1002/nbm.1210

Oeltzschner, G., Saleh, M. G., Rimbault, D., Mikkelsen, M., Chan, K. L., Puts, N. A., & Edden, R. A. (2019). Advanced Hadamard-encoded editing of seven low-concentration brain metabolites: Principles of HERCULES. *Neuroimage*, *185*, 181-190.

Oeltzschner, G., Zöllner, H. J., Hui, S. C., Mikkelsen, M., Saleh, M. G., Tapper, S., & Edden, R. A. (2020). Osprey: Open-source processing, reconstruction & estimation of magnetic resonance spectroscopy data. *Journal of neuroscience methods*, *343*, 108827.

Ogoh, S., Sato, K., Nakahara, H., Okazaki, K., Subudhi, A. W., & Miyamoto, T. (2013). Effect of acute hypoxia on blood flow in vertebral and internal carotid arteries. *Experimental physiology*, *98*(3), 692-698.

Pamenter, M. E., & Powell, F. L. (2016). Time Domains of the Hypoxic Ventilatory Response and Their Molecular Basis. *Comprehensive Physiology*, *6*(3), 1345–1385. https://doi.org/10.1002/cphy.c150026

Pelli, D.G., (1997). The VideoToolbox software for visual psycho- physics: transforming numbers into movies. Spat Vis; 10: 437–442.

Pfefferbaum, A., Chanraud, S., Pitel, A. L., Müller-Oehring, E., Shankaranarayanan, A., Alsop, D. C., ... & Sullivan, E. V. (2011). Cerebral blood flow in posterior cortical nodes of the default mode network decreases with task engagement but remains higher than in most brain regions. *Cerebral cortex*, *21*(1), 233-244.

Posse, S., Olthoff, U., Weckesser, M., Jäncke, L., Müller-Gärtner, H. W., & Dager, S. R. (1997). Regional dynamic signal changes during controlled hyperventilation assessed with blood oxygen level-dependent functional MR imaging. *American journal of neuroradiology*, *18*(9), 1763-1770.

Prakash, R. S., Heo, S., Voss, M. W., Patterson, B., & Kramer, A. F. (2012). Age-related differences in cortical recruitment and suppression: implications for cognitive performance. *Behavioural brain research*, *230*(1), 192-200.

oulin, M. J., & Robbins, P. A. (1998). Influence of cerebral blood flow on the ventilatory response to hypoxia in humans. *Experimental physiology*, *83*(1), 95-106.

Rae, C. D. (2014). A guide to the metabolic pathways and function of metabolites observed in human brain 1 H magnetic resonance spectra. *Neurochemical research*, *39*, 1-36.

Rae, C. D., & Williams, S. R. (2017). Glutathione in the human brain: Review of its roles and measurement by magnetic resonance spectroscopy. *Analytical biochemistry*, *529*, 127-143.

Raichle, M. E. (2015). The brain's default mode network. *Annual review of neuroscience*, *38*, 433-447.

Raichle, M. E., MacLeod, A. M., Snyder, A. Z., Powers, W. J., Gusnard, D. A., & Shulman, G. L. (2001). A default mode of brain function. *Proceedings of the national academy of sciences*, *98*(2), 676-682.

Richalet, J. P., Souberbielle, J. C., Antezana, A. M., Dechaux, M., Le Trong, J. L., Bienvenu, A, ... & Zittoun, J. (1994). Control of erythropoiesis in humans during prolonged

exposure to the altitude of 6,542 m. *American Journal of Physiology-Regulatory, Integrative and Comparative Physiology*, *266*(3), R756-R764.

Rijpma, A., van der Graaf, M., Meulenbroek, O., Rikkert, M. G. O., & Heerschap, A. (2018). Altered brain high-energy phosphate metabolism in mild Alzheimer's disease: A 3-dimensional 31P MR spectroscopic imaging study. *NeuroImage: Clinical*, *18*, 254-261.

Rhencrona, S. (1985). Brain acidosis. Annals of Emergency Medicine, 14(8), 770-776. https://doi.org/10.1016/S0196-0644(85)80055-X

Roach, R.C., Hackett, P.H., Oelz, O., Bartsch, P., Luks, A.M., MacInnis, M.J., Baillie, J.K., & The Lake Louise AMS Score Consensus Committee (2018). The 2018 lake louise acute mountain sickness score. *High Altitude Medicine and Biology*, *19*(1), 4-6. doi: 10.1089/ham.2017.0164

Rogan, M., Friend, A. T., Rossetti, G. M., Edden, R., Mikkelsen, M., Oliver, S. J., ... & Mullins, P. G. (2022). Hypoxia alters posterior cingulate cortex metabolism during a memory task: a 1H fMRS study. *Neuroimage*, *260*, 119397.

Rossetti, G. M. K., d'Avossa, G., Rogan, M., Macdonald, J. H., Oliver, S. J., & Mullins, P. G. (2020). Reversal of neurovascular coupling in the default mode network: Evidence from hypoxia. *Journal of Cerebral Blood Flow and Metabolism*. https://doi.org/10.1177/0271678X20930827

Rossion, B., & Pourtois, G. (2004). Revisiting Snodgrass and Vanderwart's object pictorial set: The role of surface detail in basic-level object recognition. *Perception*, *33*(2), 217-236.

RStudio Team (2020). RStudio: Integrated Development Environment for R. RStudio, PBC, Boston, MA. Available from http://www.rstudio.com/

Saleh, M. G., Rimbault, D., Mikkelsen, M., Oeltzschner, G., Wang, A. M., Jiang, D., ... & Edden, R. A. (2019). Multi-vendor standardized sequence for edited magnetic resonance spectroscopy. *Neuroimage*, *189*, 425-431.

Schaller, B., Xin, L., O'Brien, K., Magill, A. W., & Gruetter, R. (2014). Are glutamate and lactate increases ubiquitous to physiological activation? A 1H functional MR spectroscopy study during motor activation in human brain at 7Tesla. *NeuroImage*, *93*(P1), 138–145. https://doi.org/10.1016/j.neuroimage.2014.02.016

Schlünzen, L., Vafaee, M. S., Juul, N., & Cold, G. E. (2010). Regional cerebral blood flow responses to hyperventilation during sevoflurane anaesthesia studied with PET. *Acta anaesthesiologica scandinavica*, *54*(5), 610-615.

Scremin, O. U., & Jenden, D. J. (1993). Acetylcholine turnover and release: the influence of energy metabolism and systemic choline availability. *Progress in Brain Research*, *98*, 191-195.

Seeley, W. W., Crawford, R. K., Zhou, J., Miller, B. L., & Greicius, M. D. (2009). Neurodegenerative diseases target large-scale human brain networks. *Neuron*, *62*(1), 42-52.

Semenza, G. L., Nejfelt, M. K., Chi, S. M., & Antonarakis, S. E. (1991). Hypoxia-inducible nuclear factors bind to an enhancer element located 3'to the human erythropoietin gene. *Proceedings of the National Academy of Sciences*, *88*(13), 5680-5684.

Singmann, H. (2018). Afex: Analysis of Factorial Experiments [computer software]. Retrieved from: https://cran.r-project.org/package=afex.

Shapiro, W., Wasserman, A. J., Baker, J. P., & Patterson, J. L. (1970). Cerebrovascular response to acute hypocapnic and eucapnic hypoxia in normal man. *The Journal of clinical investigation*, *49*(12), 2362-2368.

Sharp, F. R., & Bernaudin, M. (2004). HIF1 and oxygen sensing in the brain. *Nature Reviews Neuroscience*, *5*(6), 437-448.

Smith, S. M. (2002). Fast robust automated brain extraction. *Human brain mapping*, *17*(3), 143-155.

Smith, Z. M., Krizay, E., Guo, J., Shin, D. D., Scadeng, M., & Dubowitz, D. J. (2013). Sustained high-altitude hypoxia increases cerebral oxygen metabolism. *Journal of Applied Physiology*, *114*(1), 11-18.

Snyder, J., & Wilman, A. (2010). Field strength dependence of PRESS timings for simultaneous detection of glutamate and glutamine from 1.5 to 7 T. *Journal of magnetic resonance*, *203*(1), 66-72.

Soares, D. P., & Law, M. (2009). Magnetic resonance spectroscopy of the brain: review of metabolites and clinical applications. *Clinical radiology*, *64*(1), 12-21.

Stanley, J. A., & Raz, N. (2018). Functional magnetic resonance spectroscopy: The "new" MRS for cognitive neuroscience and psychiatry research. *Frontiers in Psychiatry*. https://doi.org/10.3389/fpsyt.2018.00076

Stagg, C. J., Bachtiar, V., & Johansen-Berg, H. (2011). What are we measuring with GABA magnetic resonance spectroscopy?. *Communicative & integrative biology*, *4*(5), 573-575.

Stefan, D. D. C. F., Di Cesare, F., Andrasescu, A., Popa, E., Lazariev, A., Vescovo, E., ... & Graveron-Demilly, D. (2009). Quantitation of magnetic resonance spectroscopy

signals: the jMRUI software package. *Measurement Science and Technology*, *20*(10), 104035.

Steinback, C. D., & Poulin, M. J. (2007). Ventilatory responses to isocapnic and poikilocapnic hypoxia in humans. *Respiratory physiology & neurobiology*, *155*(2), 104-113.

Steinback, C. D., & Poulin, M. J. (2008). Cardiovascular and cerebrovascular responses to acute isocapnic and poikilocapnic hypoxia in humans. *Journal of Applied Physiology*, *104*(2), 482-489.

Steinback, C. D., & Poulin, M. J. (2016). Influence of hypoxia on cerebral blood flow regulation in humans. *Hypoxia: Translation in Progress*, 131-144.

Swenson, E. R. (2016). Hypoxia and its acid–base consequences: from mountains to malignancy. *Hypoxia: Translation in Progress*, 301-323.

Tabata, M., Kurosawa, H., Kikuchi, Y., Hida, W., Ogawa, H., Okabe, S., ... & Shirato, K. (2001). Role of GABA within the nucleus tractus solitarii in the hypoxic ventilatory decline of awake rats. *American Journal of Physiology-Regulatory, Integrative and Comparative Physiology*, *281*(5), R1411-R1419.

Tagamets, M. A., & Horwitz, B. (2001). Interpreting PET and fMRI measures of functional neural activity: the effects of synaptic inhibition on cortical activation in human imaging studies. *Brain research bulletin*, *54*(3), 267-273.

Takado, Y., Takuwa, H., Sampei, K., Urushihata, T., Takahashi, M., Shimojo, M., ... & Higuchi, M. (2022). MRS-measured glutamate versus GABA reflects excitatory versus inhibitory neural activities in awake mice. *Journal of Cerebral Blood Flow & Metabolism*, *42*(1), 197-212.

Terraneo, L., & Samaja, M. (2017). Comparative response of brain to chronic hypoxia and hyperoxia. *International journal of molecular sciences*, *18*(9), 1914.

Tissot van Patot, M. C., & Gassmann, M. (2011). Hypoxia: adapting to high altitude by mutating EPAS-1, the gene encoding HIF-2α. *High altitude medicine & biology*, *12*(2), 157-167.

Thomas, K. N., Lewis, N. C., Hill, B. G., & Ainslie, P. N. (2015). Technical recommendations for the use of carotid duplex ultrasound for the assessment of extracranial blood flow. *American Journal of Physiology-Regulatory, Integrative and Comparative Physiology*, *309*(7), R707-R720.

Turner, C. E., Byblow, W. D., & Gant, N. (2015). Creatine supplementation enhances corticomotor excitability and cognitive performance during oxygen deprivation. *Journal of Neuroscience*, *35*(4), 1773-1780.

Ulus, I. H., Wurtman, R. J., Mauron, C., & Blusztajn, J. K. (1989). Choline increases acetylcholine release and protects against the stimulation-induced decrease in phosphatide levels within membranes of rat corpus striatum. *Brain research*, *484*(1-2), 217-227.

Van De Ven, K., & Keupp, J. (2018). Amide Proton Transfer weighted imaging: Advancements in molecular tumour diagnosis. Retrieved from: https://www.philips.co.uk/healthcare/resources/landing/the-next-mr-wave/3d-apt

Van Zijl, P. C., & Yadav, N. N. (2011). Chemical exchange saturation transfer (CEST): what is in a name and what isn't?. *Magnetic resonance in medicine*, *65*(4), 927-948.

Vepraskas, S., Toth, H., & Weisgerber, M. (2023). 59—Acid–Base and Electrolyte Disturbances. In R. M. Kliegman, H. Toth, B. J. Bordini, & D. Basel (Eds.), *Nelson Pediatric Symptom-Based Diagnosis: Common Diseases and their Mimics (Second Edition)* (Second Edition, pp. 1114-1138.e2). Elsevier. https://doi.org/10.1016/B978-0-323-76174-1.00059-6

Vestergaard, M. B., Ghanizada, H., Lindberg, U., Arngrim, N., Paulson, O. B., Gjedde, A., ... & Larsson, H. B. (2022). Human cerebral perfusion, oxygen consumption, and lactate production in response to hypoxic exposure. *Cerebral Cortex*, *32*(6), 1295-1306.

Vestergaard, M. B., & Larsson, H. B. (2019). Cerebral metabolism and vascular reactivity during breath-hold and hypoxic challenge in freedivers and healthy controls. *Journal of Cerebral Blood Flow & Metabolism*, *39*(5), 834-848. DOI: 10.1177/0271678X17737909

Vestergaard, M. B., Lindberg, U., Aachmann-Andersen, N. J., Lisbjerg, K., Christensen, S. J., Law, I., … Larsson, H. B. W. (2016). Acute hypoxia increases the cerebral metabolic rate-a magnetic resonance imaging study. *Journal of Cerebral Blood Flow and Metabolism*, *36*(6), 1046–1058. https://doi.org/10.1177/0271678X15606460

Vogt, B. A., & Laureys, S. (2005). Posterior cingulate, precuneal and retrosplenial cortices: cytology and components of the neural network correlates of consciousness. *Progress in brain research*, *150*, 205-217.

Wang, K., Smith, Z. M., Buxton, R. B., Swenson, E. R., & Dubowitz, D. J. (2015). Acetazolamide during acute hypoxia improves tissue oxygenation in the human brain. *Journal of Applied Physiology*, *119*(12), 1494-1500.

Ward, K. M., & Balaban, R. S. (2000). Determination of pH using water protons and chemical exchange dependent saturation transfer (CEST). *Magnetic Resonance in Medicine: An Official Journal of the International Society for Magnetic Resonance in Medicine*, *44*(5), 799-802.

Wickham, H., Averick, M., Bryan, J., Chang, W., D'Agostino McGowan, L., François, R.,… Yutani, H. (2019). Welcome to the tidyverse. Journal of Open Source Software, 4(43), 1686. Available from https://doi.org/10.21105/joss.01686

Wijtenburg, S. A., & Knight-Scott, J. (2011). Very short echo time improves the precision of glutamate detection at 3T in 1H magnetic resonance spectroscopy. *Journal of Magnetic Resonance Imaging*, *34*(3), 645-652.

Williams, T. B., Corbett, J., McMorris, T., Young, J. S., Dicks, M., Ando, S., … Costello, J. T. (2019). Cognitive performance is associated with cerebral oxygenation and peripheral oxygen saturation, but not plasma catecholamines, during graded normobaric hypoxia. *Experimental Physiology*, *104*(9), 1384–1397. https://doi.org/10.1113/EP087647

Willie, C. K., Macleod, D. B., Shaw, A. D., Smith, K. J., Tzeng, Y. C., Eves, N. D., ... & Ainslie, P. N. (2012). Regional brain blood flow in man during acute changes in arterial blood gases. *The Journal of physiology*, *590*(14), 3261-3275.

Willie, C. K., Tzeng, Y. C., Fisher, J. A., & Ainslie, P. N. (2014). Integrative regulation of human brain blood flow. *Journal of Physiology*, *592*(5), 841–859. https://doi.org/10.1113/jphysiol.2013.268953

Winkler, A. M., Ridgway, G. R., Webster, M. A., Smith, S. M., & Nichols, T. E. (2014). Permutation inference for the general linear model. *Neuroimage*, *92*, 381-397.

Wolff, H. G., Lennox, W. G., & Allen, M. B. (1930). Cerebral circulation: XII. The effect on pial vessels of variations in the oxygen and carbon dioxide content of the blood. *Archives of Neurology & Psychiatry*, *23*(6), 1097-1120.

Xu, F., Liu, P., Pascual, J. M., Xiao, G., & Lu, H. (2012). Effect of hypoxia and hyperoxia on cerebral blood flow, blood oxygenation, and oxidative metabolism. *Journal of Cerebral Blood Flow & Metabolism*, *32*(10), 1909-1918.

Yamada, H., Sadato, N., Konishi, Y., Muramoto, S., Kimura, K., Tanaka, M., ... & Itoh, H. (2000). A milestone for normal development of the infantile brain detected by functional MRI. *Neurology*, *55*(2), 218-223.

Yar, R. A., Akbar, A., & Iqbal, F. (2015). Creatine monohydrate supplementation for 10 weeks mediates neuroprotection and improves learning/memory following neonatal

hypoxia ischemia encephalopathy in female albino mice. *brain research*, *1595*, 92-100.

Zhang, Y., Brady, M., & Smith, S. (2001). Segmentation of brain MR images through a hidden Markov random field model and the expectation-maximization algorithm. *IEEE transactions on medical imaging*, *20*(1), 45-57.

Zhang, D., & Raichle, M. E. (2010). Disease and the brain's dark energy. *Nature Reviews Neurology*, *6*(1), 15-28.

Zheng, Y., & Wang, X. M. (2017). Measurement of lactate content and amide proton transfer values in the basal ganglia of a neonatal piglet hypoxic-ischemic brain injury model using MRI. *American Journal of Neuroradiology*, *38*(4), 827-834.

Zhou, J., Payen, J. F., Wilson, D. A., Traystman, R. J., & Van Zijl, P. C. (2003). Using the amide proton signals of intracellular proteins and peptides to detect pH effects in MRI. *Nature medicine*, *9*(8), 1085-1090.

Appendix F

	Quantified_spectrum	*Normoxia*	*stdev*	*N*	*Hypoxia*	*stdev*	*N*	*Diff*	*%diff N-H*	*P-value*
Asc	sum	0.08	0.18	6	0.11	0.25	4	-0.03	-35.85	0.72
Asp	sum	2.13	0.51	13	1.82	0.55	13	0.32	14.82	0.13
Cr	sum	8.22	0.91	13	7.12	0.98	13	1.10	13.42	0.00
GABA	diff1	2.66	0.37	13	3.34	0.64	13	-0.68	-25.65	0.01
GABA+	diff1	5.54	0.59	13	5.89	1.01	13	-0.35	-6.35	0.30
GPC	sum	0.92	0.45	13	1.03	0.39	13	-0.11	-12.09	0.50
GSH	diff2	3.12	0.66	13	3.10	0.44	13	0.02	0.76	0.91
Gln	diff1	2.29	0.80	13	1.57	0.59	13	0.71	31.17	0.00
Glu	sum	12.02	1.31	13	11.12	2.21	13	0.90	7.53	0.14
mI	sum	6.94	0.77	13	6.26	1.01	13	0.67	9.71	0.01
Lac	diff2	0.97	0.20	13	1.26	0.25	13	-0.29	-29.46	0.00
NAA	sum	16.60	0.98	13	15.63	1.39	13	0.97	5.86	0.02
NAAG	sum	2.63	0.52	13	2.91	0.69	13	-0.28	-10.74	0.25
PCh	sum	1.18	0.45	13	0.88	0.50	12	0.30	25.32	0.11
PCr	sum	3.86	1.10	13	4.17	0.65	13	-0.31	-8.07	0.37
PE	diff2	5.12	0.78	13	4.28	0.95	13	0.84	16.42	0.01
sI	sum	0.25	0.17	13	0.24	0.14	13	0.01	2.41	0.79
Tau	sum	2.73	0.68	13	2.07	0.65	13	0.66	24.05	0.00
MM09	sum	1.13	0.67	13	1.13	0.40	13	0.00	0.01	1.00
MM12	sum	0.68	0.54	11	0.95	0.77	12	-0.27	-39.86	0.38
MM14	sum	2.62	1.14	13	3.13	1.05	13	-0.51	-19.66	0.18
MM17	sum	0.97	0.71	12	0.75	0.83	10	0.22	22.25	0.56
MM20	sum	1.19	0.55	13	1.30	0.60	13	-0.11	-8.90	0.61
Lip09	sum	2.39	1.11	13	2.78	1.08	13	-0.38	-16.03	0.34
Lip13	sum	1.29	0.93	12	1.65	1.03	12	-0.36	-27.81	0.44
Lip20	sum	0.50	0.62	7	0.29	0.50	6	0.21	42.15	0.32
tNAA	sum	19.97	1.00	13	19.18	1.73	13	0.80	3.98	0.10
Glx	sum	11.94	1.32	13	10.90	2.14	13	1.03	8.67	0.09
tCho	sum	2.07	0.12	13	1.88	0.18	13	0.18	8.95	0.00
tCr	sum	12.08	0.66	13	11.29	0.91	13	0.79	6.55	0.01

Appendix G

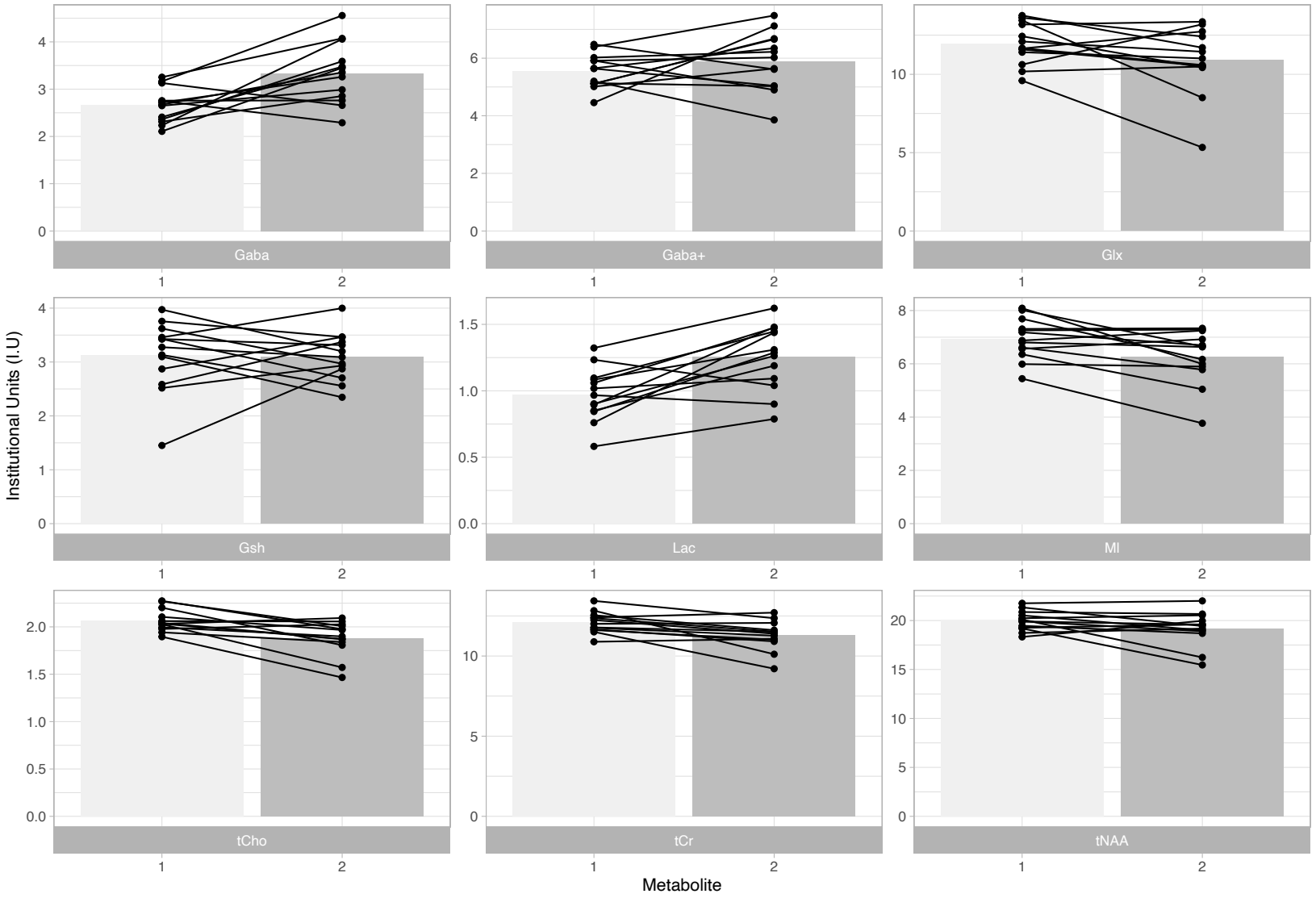
Institutional Units (I.U)
Gaba
Gaba+
Glx
Gsh
Lac
MI
tCho
tCr
tNAA
Metabolite

Appendix H

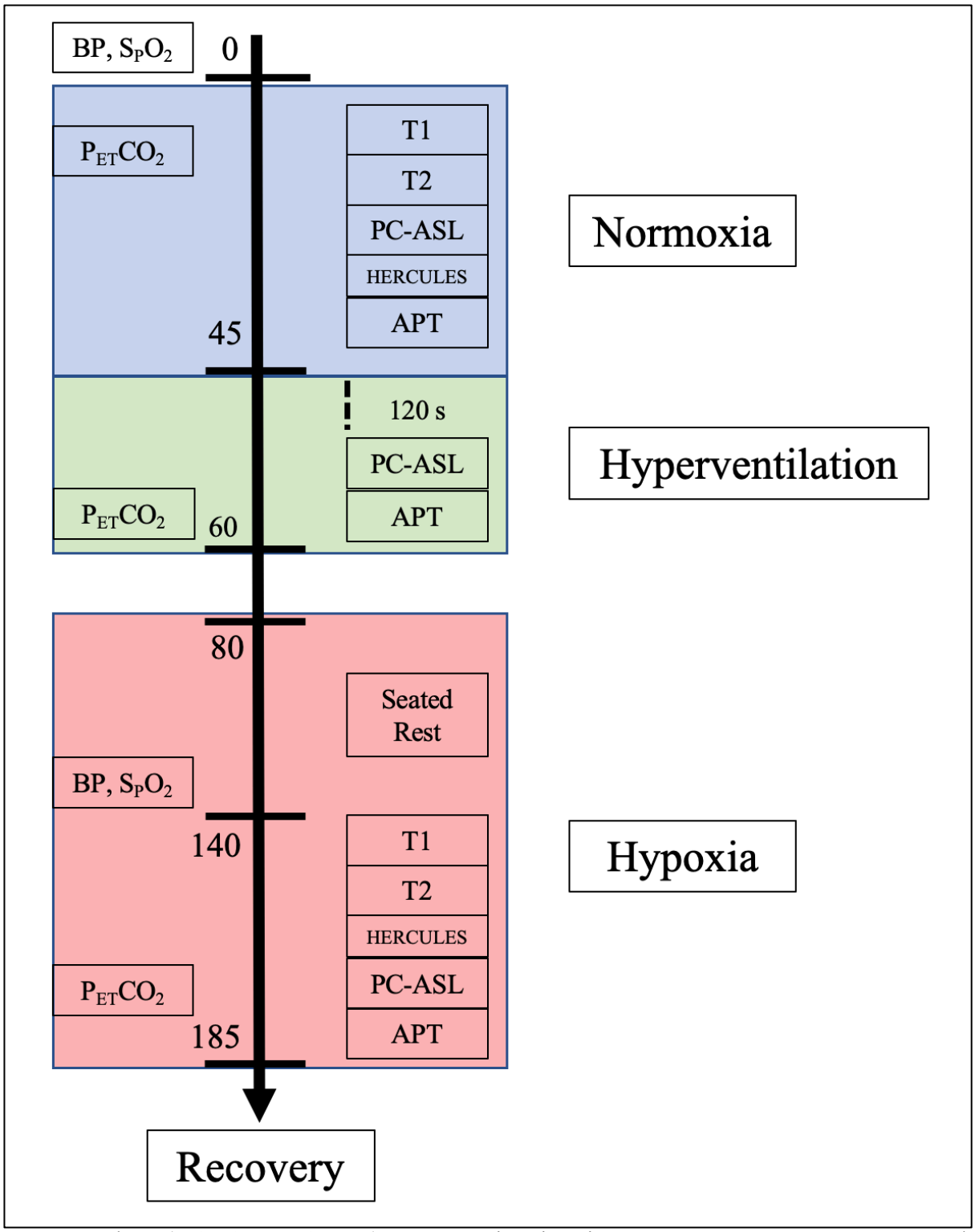

Note. Numbers (0,45,60,80,140,185) represent time in minutes. 120 s represents a 120 second adjustment period to enhanced breathing before MR acquisition commenced. Peripheral arterial oxygen saturation (SpO_2), Partial pressure of end tidal carbon dioxide ($P_{ET}CO_2$) and blood pressure (BP). T_1-weighted images (T1).). T_2-weighted images (T2). Hadamard Editing Resolves Chemicals Using Linear-combination Estimation of Spectra (HURCULES). Pseudo continuous Arterial Spin Labelling (PC-ASL). Amide Proton Transfer Imaging (APT).

Appendix I

Glasgow Coma Scale (GCS)

Add together the individual scores for each symptom to get the total score.

Eye Opening	Spontaneous	**4**
	To sound	**3**
	To pressure	**2**
	None	**1**
	Not Testable	**NT**
Verbal Response	Orientated	**5**
	Confused	**4**
	Words, but not coherent	**3**
	Sounds, but no words	**2**
	None	**1**
	Not Testable	**NT**
Motor Response	Obeys command	**6**
	Localizing	**5**
	Normal flexion	**4**
	Abnormal flexion	**3**
	Extension	**2**
	None	**1**
	Not Testable	**NT**

A GCQ <15 or any sign of HAPE/HACE

HACE – High Altitude Cerebral Oedema

- Confusion
- Fatigue
- Ataxia (Balance)
- Difficulty Speaking
- Unusual Behaviour
- Vomiting
- Hallucinations
- Blindness
- Seizures
- Unconsciousness
- Paralysis
- Coma

HAPE – High Altitude Pulmonary Oedema

- Difficulty breathing at rest
- Cough
- Congestion
- Weakness
- Crackles or wheezing while breathing
- Cyanosis
- Tachycardia (irregular)
- Tachypnea

If you are ever unsure about whether it is safe to leave a participant in the chamber, just remove them

Appendix J

Lake Louise Questionnaire (LLQ)

A diagnosis of acute mountain sickness (AMS) is based on the following conditions;

- Exposure to altitude within the last 4 days
- Presence of a headache

AND

- Presence of at least one other symptom
- A total of 3 of more

SELF-REPORT QUESTIONNAIRE

Add together the individual scores for each symptom to get the total score.

Headache	No headache	**0**
	Mild headache	**1**
	Moderate headache	**2**
	Severe headache	**3**
Gastrointestinal symptoms	None	**0**
	Poor appetite or nausea	**1**
	Moderate nausea or vomiting	**2**
	Severe nausea or vomiting	**3**
Fatigue and weakness	Not tired or weak	**0**
	Mild fatigue/weakness	**1**
	Moderate fatigue/weakness	**2**
	Severe fatigue/weakness	**3**
Dizziness/light-headedness	Not dizzy	**0**
	Mild dizziness	**1**
	Moderate dizziness	**2**
	Severe dizziness, incapacitating	**3**

A total LLQ score of 5 or more, with the presence of headache, and at least one other symptom, the participant must be removed for the chamber/Douglas bag

If you are ever unsure about whether it is safe to leave a participant in the chamber, just remove them

Appendix K

Condition	Pre-hypoxia	Hyperventilation	Hypoxia
SpO_2	98 (1)	-	85 (4)
HR	71 (10)	-	82 (14)
MAP	86 (7)	-	86 (6)
$P_{ET}CO_2$	42 (5)	33 (7)	37 (15)

Note. Peripheral arterial oxygen saturation (SpO_2), Heart Rate (HR), Mean Arterial Pressure (MAP), Partial pressure of end tidal carbon dioxide ($P_{ET}CO_2$). Values in () represent the standard deviation of the above mean value.